Acta Pharmaceutica Sinica B 2024;14(5):2057−2076

Chinese Pharmaceutical Association
Institute of Materia Medica, Chinese Academy of Medical Sciences

Acta Pharmaceutica Sinica B

www.elsevier.com/locate/apsb
www.sciencedirect.com

ORIGINAL ARTICLE

The raphe nuclei are the early lesion site of gastric α-synuclein propagation to the substantia nigra

Chenglu Zhang[†], **Ruxue Bo**[†], **Tiantian Zhou, Naihong Chen**[*], **Yuhe Yuan**[*]

State Key Laboratory of Bioactive Substances and Functions of Natural Medicines, Chinese Academy of Medical Sciences & Peking Union Medical College Institute of Materia Medica, Beijing 100050, China

Received 23 September 2023; received in revised form 14 December 2023; accepted 5 January 2024

KEY WORDS

Raphe nuclei;
α-Synuclein;
Gastrointestinal tract;
Electrophysiology;
Locus coeruleus;
Substantia nigra pars compacta;
Parkinson's disease;
Spinal cord

Abstract Parkinson's disease (PD) is a neurodegeneration disease with α-synuclein accumulated in the substantia nigra pars compacta (SNpc) and most of the dopaminergic neurons are lost in SNpc while patients are diagnosed with PD. Exploring the pathology at an early stage contributes to the development of the disease-modifying strategy. Although the "gut−brain" hypothesis is proposed to explain the underlying mechanism, where the earlier lesioned site in the brain of gastric α-synuclein and how α-synuclein further spreads are not fully understood. Here we report that caudal raphe nuclei (CRN) are the early lesion site of gastric α-synuclein propagating through the spinal cord, while locus coeruleus (LC) and substantia nigra pars compacta (SNpc) were further affected over a time frame of 7 months. Pathological α-synuclein propagation *via* CRN leads to neuron loss and disordered neuron activity, accompanied by abnormal motor and non-motor behavior. Potential neuron circuits are observed among CRN, LC, and SNpc, which contribute to the venerability of dopaminergic neurons in SNpc. These results show that CRN is the key region for the gastric α-synuclein spread to the midbrain. Our study provides valuable details for the "gut−brain" hypothesis and proposes a valuable PD model for future research on early PD intervention.

*Corresponding authors.
E-mail addresses: chennh@imm.ac.cn (Naihong Chen), yuanyuhe@imm.ac.cn (Yuhe Yuan).
[†]These authors made equal contributions to this work.

Peer review under the responsibility of Chinese Pharmaceutical Association and Institute of Materia Medica, Chinese Academy of Medical Sciences.

https://doi.org/10.1016/j.apsb.2024.01.015

1. Introduction

Parkinson's disease (PD) is a neurodegeneration disease marked by the loss of dopaminergic neurons in the substantia nigra pars compacta (SNpc)[1]. The accumulated α-synuclein is the pathological marker of PD and α-synuclein propagation promotes the disease progression[2,3]. Dopaminergic drugs are the most common medication in clinical for motor symptoms. However, dopaminergic drugs have some adverse reactions and complications, and yet cannot halt the spread of α-synuclein and disease progress[4]. The underlying mechanism of early PD remains unclear, which makes the development of disease-modifying drugs challenging. Therefore, preventing α-synuclein from spreading at an early stage and protecting the dopaminergic neurons before being affected by pathological α-synuclein may be disease-modifying. Research indicates that α-synuclein accumulates in several brain regions before it is deposited and damages neurons in SNpc. In stage 2 of the Braak stages, aggregated α-synucleins were found in caudal raphe nuclei (CRN), LC and other regions of the brain stem[5]. It is hypothesized that aggregated α-synuclein starts in the gastrointestinal tract and then spreads to the brain[6]. Research indicated that gastrointestinal α-synuclein propagated through the vagus nerve and caused pathological changes in the brain stem, locus coeruleus (LC), and SNpc[7–9]. However, which region in the brain stem was the earlier lesion site by gastric α-synuclein remains unknown. And the correlation among CRN, LC, and SNpc needs further investigation.

Raphe nuclei (RN) are located in the midline of the intermediate reticular zone and consist mostly of serotoninergic neurons[10]. Rostral RN is located in the midbrain and upper pons and secretes most of the serotonin. While CRN is located in the lower pons and medulla and consists of several nuclei, including raphe magnus (RMg), raphe obscurus (ROb), and raphe pallidus (RPa)[10,11]. Clinical studies showed that the serotonin transporter in RN was damaged in PD patients at an early stage[12,13]. The lesions in CRN are also related to motor and non-motor symptoms in PD. The serotoninergic neuron dysfunction is associated with the severity of motor deficits[12]. The higher binding of serotonin transporter was observed in PD patients. The higher binding may be due to the lower extracellular serotonin levels in CRN and related to PD depression[14]. The rapid-eye-movement (REM) sleep disorder (RBD) is considered a non-motor symptom at the prodromal stage of PD. CRN neuron dysfunction contributes to the atonia of REM sleep[15]. Clinical research demonstrated neuron loss and pathological α-synuclein in CRN of RBD patients. And most of those patients subsequently developed Lewy body disorder, like PD[16]. These results further highlight the importance of CRN pathology at an early stage in PD progression.

In this study, we showed that CRN was the key region of gastric α-synuclein propagating to the midbrain. The gastric α-synuclein propagated upward to the CRN through the spinal cord, further damaged LC and SNpc through the CRN neurons, and triggered PD-like symptoms. The long projection of CRN neurons propagated pathological α-synuclein to LC and SNpc. Furthermore, CRN α-synuclein led to motor and non-motor disorders, with progressive accumulation and phosphorylation of α-synuclein. CRN α-synuclein also led to an increase of gastric α-synuclein, further forming a vicious circle. Here, we highlight the novel strategies for the potential disease-modifying strategy: preventing α-synuclein from propagating and aggregating through CRN may delay the further lesions on the dopaminergic neurons in SNpc, and maintain the homeostasis of serotonergic neurons and its long projection to SNpc may help to protect dopaminergic neurons at an early stage.

2. Materials and methods

2.1. Animals

A total of 70 wild-type male C57BL/6N (19−21 g) mice were used in this study. All mice were purchased from Charles River Co. of China (Beijing, China). Mice were housed under 12 h light/dark cycle and had free access to food and water. After one week of adaption, mice were used in the experiments. All the animal experiments followed the guidelines of the Care and Use of Laboratory animals (United States National Institutes of Health) for the care and use of laboratory animals. The experiments were approved by the Animal Care & Welfare Committee of Institute of Materia Medica, CAMS&PUMC (Beijing, China).

2.2. Adeno-associated viral (AAV) vector injection

In this study, we used adeno-associated viral (AAV) vectors to overexpress human α-synuclein. AAV9-CMV bGloin-MCS-SNCA-3Flag-SV40 PolyA (SNCA), 5.3×10^{13} vg/mL, was used for stomach injection. AAV9-CMV bGlobin-MCS-SNCA-EGFP-3FLAG-WPRE-hGH polyA (SNCA-EGFP), 1.87×10^{13} vg/mL, was used in intracranial stereotactic injection. AAV2/9-TPH2-mCherry-WPRE-hGH pA (TPH2-mCherry), 2.00×10^{12} vg/mL, was used for DR and CRN injection. The vectors were constructed by Shanghai Genechemical Corporation (Shanghai, China).

For SNCA injection in the muscle layer of the glandular stomach, mice were anesthetized with isoflurane. Three equidistant spots in the mucous muscle layer of the gastric gland were chosen. Each site was injected with 1 μL of SNCA or negative control vectors in 3 min.

For SNCA-EGFP intracranial stereotactic injection, mice were anesthetized with isoflurane. A total volume of 1 μL vectors was stereotactically injected into the ROb using a microinjector in 5 min. The coordinates are AP −0.64 cm and DV −0.55 cm relative to Bregma.

For TPH2-mCherry intracranial stereotactic injection, mice were anesthetized with isoflurane. A total volume of 1 μL vectors was stereotactically injected into the ROb or DR using a microinjector in 5 min. The coordinates are ROb: AP −0.64 cm, DV −0.55 cm; DR: AP −0.44 cm, DV −0.3 cm relative to Bregma.

2.3. Tissue preparation

For tissue preparation, mice were anesthetized with isoflurane. Then mice were perfused transcardially with 0.1 mol/L phosphate-buffered saline (PBS) followed by 4% paraformaldehyde (PFA). Brain and gastrointestinal tract samples were post-fixed in 4% PFA for 2 days and then dehydrated in 10%, 20%, and 30% sucrose-paraformaldehyde solution for 2 days separately. For immunostaining, brains were cut into 12 μm or 20 μm coronal sections using a freezing microtome (Leica CM3050 S, Nussloch, Germany). Sections were fixed on adhesion microscope slides and

stored at −20 °C. For total protein extraction, the tissues were prepared as described previously[17]. Tissues were homogenized with RIPA lysis buffer containing protease inhibitors and phosphatase inhibitors. Then the lysates were centrifuged in 12,000×*g* at 4 °C for 30 min, and the supernatant was collected. The total protein was measured by a BCA kit (P1511, Applygen, Beijing, China).

2.4. Immunochemistry

For immunochemistry, sections were first heated in citrate buffer (pH 6.0) for 10 min for antigen retrieval. After cooling, sections were washed in 0.1 mol/L PBS 3 times, 5 min each, then permeabilized with 0.5% Triton X-100 for 15 min. After washing, sections were blanched with 3% H_2O_2 for 15 min to inactive endogenous peroxidase. The sections were washed and blocked with 8% bovine serum albumin (BSA) for 30 min, followed by incubating with primary antibodies (Supporting Information Table S1) at 4 °C overnight. On the next day, the sections were first balanced to room temperate and washed in 0.1% Tween-20 in 0.1 mol/L PBS (PBS-T) for 3 times, 10 min each. Then, sections were incubated with secondary antibodies at room temperature for 2 h. Primary and secondary antibodies used in this study were listed in Table S1 and diluted by 5% BSA. After washing with PBS-T, sections were developed color with a 3,3′-diaminobenzidine (DAB) kit (G1212. Servicebio, Beijing, China). Some sections were then counterstained with hematoxylin. After dehydrating with 60%, 70%, 80%, 90%, 100% ethanol, and xylene, sections were sealed with neutral gum. Sections were examined and photographed using Olympus BX51 or Vectra 3 (PerkinElmer, USA).

For the proteinase K (PK) resistance α-synuclein immunochemistry process, 0.2 mg/mL PK (ab64220, Abcam) was used after antigen retrieval. Sections were incubated with PK at 37 °C for 30 min, then proceeded with the normal immunochemistry process.

2.5. Immunofluorescence

For immunofluorescence staining, sections proceeded with heat-mediated antigen retrieval and permeabilization. Sections were washed in PBS 3 times between each step, each time 5 min. Then, sections were blocked with 5% BSA and incubated with primary antibodies (Table S1) at 4 °C overnight. On the second day, sections were washed with PBS-T before incubating with secondary antibodies (Table S1) at room temperature for 2 h. After washing with PBS-T, sections were sealed using an anti-quench sealer (0100-01, SouthernBiotech, Birmingham, USA). Sections were examined and photographed using Leica TCS SP8X.

2.6. Western blot

For Western blot, SDS-PAGE gel and 0.45 μm polyvinylidene difluoride (PVDF) (Millipore, Darmstadt, Germany) membrane was used. After the transfer membrane, the membrane was blocked with 5% BSA or skim milk for 2 h and incubated with a specific primary antibody at 4 °C overnight. After 3 washes with TBS-T, the membrane was incubated with a second antibody at room temperature for 1 h. Then the membrane was washed with TBS-T and photographed by Tanon 4600 (Tanon, Shanghai, China). The image was analyzed by Image J.

2.7. Behavioral tests

In this study, we performed several behavioral tests at 1, 2.5, and 7 months after α-synuclein overexpression in the stomach and 3, 9, 14, and 26 weeks after α-synuclein overexpression in the CRN. The motor ability was evaluated by the grip strength test, pole test, rotarod test, and balance beam test. And non-motor deficits were assessed by open field test, elevated plus maze test, novel object recognition test, Y maze test, tail suspension test, and forced swim test[7]. All tests were conducted between 9:00−16:00 in the lights−on cycle. All the results were analyzed using GraphPad Prism 8.

2.7.1. Grip strength test

We used a grip strength test machine (YLS-13A, Shandongyiyan, China) to test the strength of the limbs of the mice. First, mice were gently put on the metal grid in the device. Second, the tail was gently pulled when the mice stably grasped the metal grid until it released the grid. The peak grip strength (g) during the process was automatically recorded. Each mouse was tested 3 times, with an interval of 30 min between each test, and the average was used for statistical analysis.

2.7.2. Pole test

The pole consisted of a 60 cm long, 1 cm diameter wooden rod with a 1.5 cm diameter ball on the top. The pole was wrapped with wool to prevent mice from slipping and fixed on a wooden base. Mice were gently placed on the ball at the top with the head facing down. And the total time taken to reach the bottom of the pole with hind limbs was recorded. All mice were trained 3 times before testing. Each mouse was tested 3 times, with an interval of 30 min between each test, and the average time was used for statistical analysis. The maximum cutoff time to stop the test was 15 s, and if the mice fell, the time was recorded as 15 s as well.

2.7.3. Rotarod test

ROTO-ROD Series 8 (IITC life science) was used in this test. Mice were trained 3 times one day in advance. For the training session, mice were gently placed on the rotarod cylinder with their head facing outside. And the speed was slowly increased from 5 to 10 rpm in 5 min. The final speed was adjusted to 30 rpm for the testing session, and each mouse was tested 3 times, with an interval of 30 min between each test. The total latency time of mice staying in the cylinder was recorded, and the average latency time was used for statistical analysis.

2.7.4. Balance beam test

We used 0.5 cm wide, 1 cm high, and 80 cm long wooden pieces as the balance beam. The balance beam was placed 40 cm high from the ground. A dark box was placed on one side while the light was placed on the other side to induce the mice to cross the balance beam. All mice were trained 3 times before testing. All mice were tested 3 times, with an interval of 30 min between each test. Mice were placed on the light side, and the total time taken to reach the dark box was recorded. The average time of 3 tests was used for statistical analysis.

2.7.5. Open field test

A 50 cm long, 50 cm wide, and 40 cm depth rectangular wooden box was used in this test. The box is covered with white paint and divided into 16 (4 × 4) identical squares. Four squares in the center were defined as the center area. Mice were gently put into

the center area of the box and allowed to explore for 5 min. The activity of each mouse during the test was recorded by an automatic tracking system (Smart 3.0). Each mouse was tested only once. The box was cleaned with 10% ethanol to remove residues and odors between each test. The total distance, entries into the center area, and time spent in the center area were measured.

2.7.6. *Elevated plus maze test*

The elevated plus-maze was a plus-shaped maze with two closed and two open arms. Both arms are 65 cm long, and 5 cm in width, and the closed arms have 15 cm walls. The maze was 40 cm in height from the ground. When performing the elevated plus-maze test, mice were placed on one side of the open arm and allowed to explore the maze for 5 min. The entries to open arms and the total time spent in open arms were recorded by a tracking system (Smart 3.0). The maze was cleaned with 10% ethanol between each test.

2.7.7. *Novel object recognition test*

The novel object recognition test was performed in the open field box. We used two 15 mL centrifuge tubes and a 25 cm^2 cell culture dish as objects and filled them with corncob. After one day of adaption to the box, mice were introduced to two identical objects and allowed to explore for 5 min. On the third day, one of the 15 mL centrifuge tubes was replaced with the 25 cm^2 cell culture dish. The time spent exploring each object was recorded by a tracking system (Smart 3.0). The novel object recognition index was calculated as Eq. (1):

$$\text{Novel object recognition index} = \text{The time spent on the novel object/The total time spent on both objects} \quad (1)$$

2.7.8. *Y maze test*

A Y maze made of plastic was used in this test. Mice were placed at the end of one arm and allowed to explore all the 3 arms freely for 8 min. The total arm entries and sequence of arm entries were recorded manually. Alternative behavior was defined as entering the three arms in succession. And the alternative index was calculated as Eq. (2):

$$\text{Alternative index (\%)} = \text{Alternative behavior/(Total arm entries}-2) \times 100 \quad (2)$$

2.7.9. *Tail suspension test*

For the tail suspension test, we suspended mice in a black box with a white background using adhesive tape attached approximately 1 cm from the tip of the tail. The trial lasted for 6 min. The immobility of mice was defined as frozen in hind limbs, and immobility time in the last 4 min was recorded manually. The adhesive tape was removed gently after the test.

2.7.10. *Forced swimming test*

We used a transparent plastic cylinder with 18 cm of water for the forced swimming test. The water temperature was 25 ± 1 °C. The mice were placed in the water for 6 min, and the immobility time in the last 4 min was recorded. The immobility in mice was defined as the mice not struggling to escape, floating on the surface, or performing only a little swim to ensure they do not sink. The cylinder was cleaned and water was changed between each test. The mice were carefully dried and maintained the body temperature after the test.

2.8. *In vivo electrophysiological test*

To detect neuronal activity, we used electrodes made of nickel-chromium to record electrical signals. The electrodes were implanted in LC and SNpc and secured with dental cement. The test was performed three to four days after recovery. The coordinates are LC: AP −0.54 cm, ML +0.0875 cm, DV −0.37 cm; SNpc: AP −0.364 cm, ML +0.12 cm, DV −0.41 cm relative to Bregma. Broadband (0.3 Hz−7.5 kHz) neural signals were recorded using a multichannel data acquisition system (Apollo 2, Bio-Signal Technologies, Nanjing, China). Spikes were extracted with high-pass (300 Hz) filters. Spike sorting was conducted by Offline Sorter (Plexon: Dallas, TX, USA). All data were analyzed using NeuroExplorer (Nex Technologies: Boston, MA, USA). Based on the properties of dopaminergic neurons, the maximum interval to start a burst was 80 ms, and 160 ms to end a burst was used in burst analysis. The minimum burst duration was 2.5 ms[18,19]. And LC cells were similarly analyzed[20].

2.9. *Statistical analysis*

The statistical analysis for immunostaining (2−4 sections per mouse per time point) was performed by Image J. First, the image was transformed to 8-bit or RGB-stack and then threshold to remark the positive area. Second, the percentage of the positive area or integrated density was measured. For Western blot analysis, first, the image was transformed to 8-bit. Then, the background was subtracted. The interested lane was selected and the integrated density was measured. All results were analyzed by GraphPad Prism 8, using two-tailed Student's *t*-test or two-way ANOVA analysis. $P < 0.05$ was considered significant.

3. Results

3.1. *α-Synuclein overexpression in the stomach led to neuron loss in CRN, LC, and SNpc*

To study the role of the stomach in the "gut−brain axis" theory, SNCA vectors were injected into the muscle layer of the glandular stomach to express full-length human α-synuclein (SNCA-stomach) (Supporting Information Fig. S1A and S1B). The mock vectors were used as the control group (Ctrl-stomach). The enteric nervous system contains diverse neurons[21] and dopaminergic neurons are widely distributed in the gastrointestinal tract. Research showed that the dopaminergic neurons are closely related to gastric pathology in PD. Clinical PD patients showed damaged dopaminergic neurons and decreased dopamine levels in the gastrointestinal tract[22−24]. So, we focused on the dopaminergic neurons in the stomach, and double immunofluorescence staining against tyrosine hydroxylase (TH) and α-synuclein showed that α-synuclein was expressed in the dopaminergic neurons after 1 month post-injection (Fig. S1C).

To confirm the early lesion site in the brain induced by gastric α-synuclein, we assessed several sites associated with Braak stages. First, the dorsal motor nucleus of the vagus (DMV) and solitary nucleus tract (NTS) in Braak stage 1 were examined. No obvious α-synuclein signal and neuronal damage were detected (Supporting Information Fig. S2A−S2C). Then, the CRN, LC, and

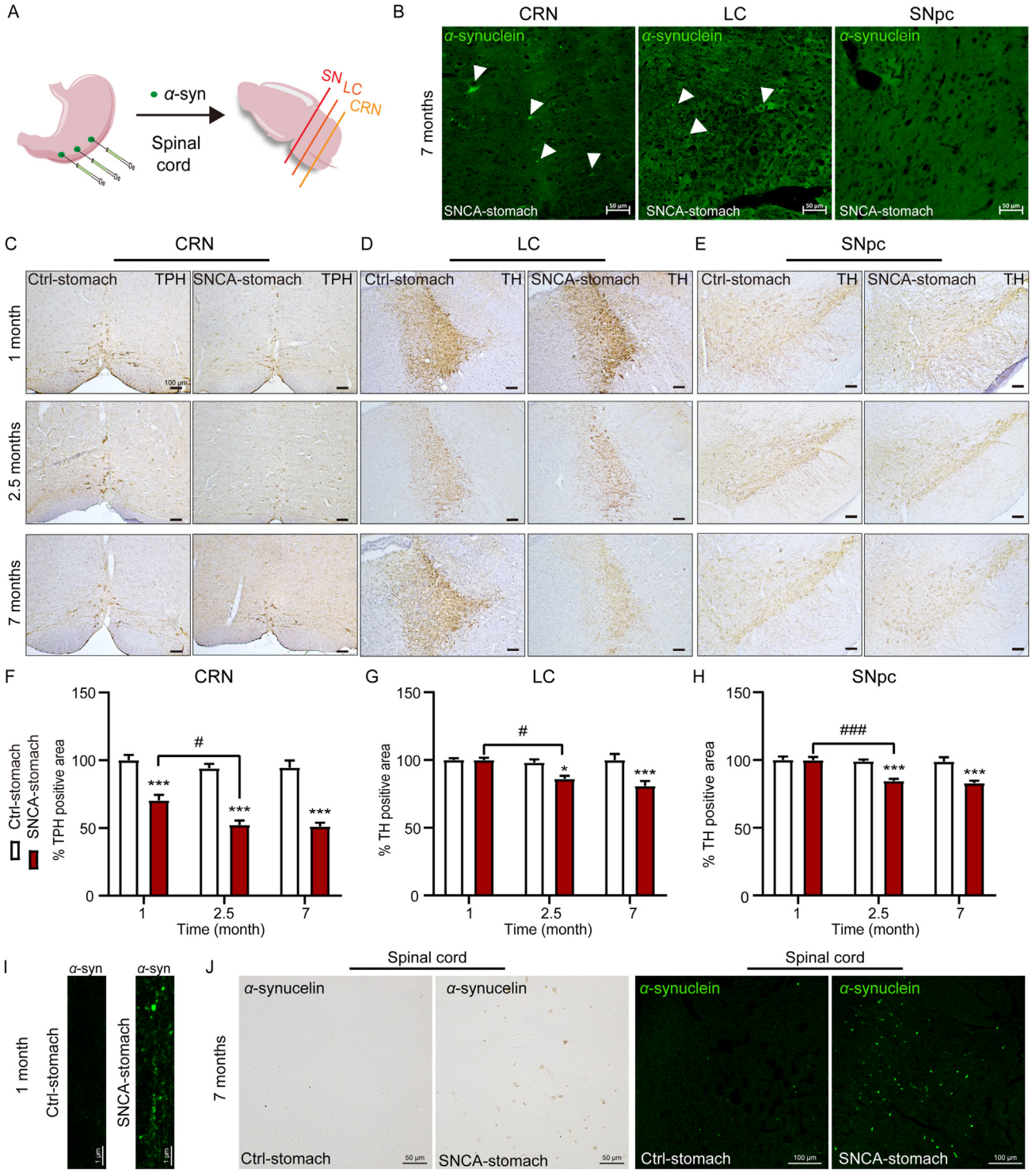

Figure 1 α-Synuclein overexpression in the stomach led to neuron loss in CRN, LC, and SNpc. (A, B) Gastric α-synuclein spread to the CRN and LC at 7 months post-injection. No obvious signal was detected in SNpc. Scale bar: 50 μm. (C−H) The representative images and quantification of TPH/TH-positive neurons in CRN (C, F), LC (D, G), and SNpc (E, H) at 1, 2.5, and 7 months post-injection. Scale bar: 100 μm. (I) The representative images of α-synuclein-positive staining of the longitudinal section of the spinal cord at 1 month post-injection. Scale bar: 1 μm. (J) The representative images of α-synuclein-positive staining of transection of the spinal cord at 7 months post-injection. Scale bar: 50 or 100 μm. Values are presented as mean ± SEM, $n = 3$, and Ctrl-stomach at 1 month was set as 100%. Two-way ANOVA followed by Tukey's *post hoc* test, $^{*}P < 0.05$, $^{***}P < 0.001$ *versus* Ctrl-stomach group; $^{\#}P < 0.05$, $^{\#\#\#}P < 0.001$ *versus* SNCA-stomach group. Abbreviations: caudal raphe nuclei (CRN), locus coeruleus (LC), substantia nigra pars compacta (SNpc).

SNpc regions were examined. The α-synuclein tagged with EGFP was observed in CRN and LC, while no signal was found in the SNpc at 7 months post-injection (Fig. 1A and B). Endogens α-synuclein was detected because pathological α-synuclein may induce prion-like propagation of endogenous α-synuclein pathology[25]. Significantly increased α-synuclein was observed in CRN, LC, and SNpc regions at 7 months post-injection in the SNCA-stomach model (Fig. S2D−S2F). Also, increased microglia were found in the SNpc (Fig. S2G). Interestingly, the serotoninergic neurons in CRN of SNCA-stomach mice were damaged significantly at 1 month post-injection, with 29.53 ± 3.98% cell loss compared to the Ctrl-stomach mice (Fig. 1C and F), while no neuron loss was observed in LC and SNpc at this time. The noradrenergic neuron loss in LC was found with 13.92 ± 2.24% cell loss at 2.5 months and 19.13 ± 3.57% at 7 months (Fig. 1D and G). Also, dopaminergic neurons in SNpc decreased significantly, with 15.42 ± 1.48% at 2.5 months and 17.06 ± 1.75% at 7 months post-injection (Fig. 1E−H). These results indicate that gastric α-synuclein induced neuron loss in CRN, LC, and SNpc and CRN was the earlier lesion site.

Since no obvious damage was observed in the DMV and NTS, which are closely related to the vagus nerve pathway[26]. The spinal cord, which is also an important route of α-synuclein propagation, was detected in the SNCA-stomach model[27]. It is interesting that much more evident stains of α-synuclein were displayed in the spinal cord of the SNCA-stomach mice (Fig. 1I and J). These results illustrate that the gastric α-synuclein might propagate through the spinal cord to the brain.

3.2. *α-Synuclein overexpression in the stomach induced PD-like behavior*

The grip strength test, rotarod test, pole test, and balance beam test were used to assess the motor deficits induced by gastric α-synuclein. Forelimb and hindlimb grip strength of SNCA-stomach mice was significantly decreased at 7 months post-injection (Fig. 2A). Similar results were observed in the rotarod test (Fig. 2B). Also, the total time taken in the pole test and balance beam test was increased at 7 months post-injection in SNCA-stomach mice (Fig. 2C and D). Taken together, gastric α-synuclein led to motor disorders in SNCA-stomach mice. Moreover, SNCA-stomach mice developed depressive-like symptoms. The immobility time of SNCA-stomach mice was increased significantly in the tail suspension test and forced swimming test at 7 months (Fig. 2E and F). No significant depression-like behavior and memory loss were found (Supporting Information Fig. S3).

3.3. *Gastric α-synuclein led to abnormal neuron firing activity in SNpc and LC*

We used *in vivo* electrophysiology to detect the firing activity of dopaminergic neurons in SNpc and noradrenergic neurons in LC at 7 months post-injection since significant motor deficits occurred at 7 months. We examined neuronal electrophysiology under anesthesia and active states, respectively. The power spectral density (PSD) was used to assess the local field potential (LFP). Firing rate, mean burst duration, mean interspike interval (ISI) in burst, and percentage of spikes in burst were analyzed to assess the firing activity.

During the pole test, the LFP of SNpc and LC neurons in the SNCA-stomach mice was increased under 40 Hz compared to Ctrl-stomach mice. No significant firing activity changes were observed in SNpc neurons. The percentage of spikes in the burst of LC neurons was increased, indicating increasing burst firing activity (Supporting Information Fig. A4A and S4B). Under anesthesia, increased LFP under 40 Hz in SNpc and LC regions of the SNCA-stomach mice was observed (Fig. S4C and S4D). The firing rate of SNpc neurons was significantly increased, while the mean burst duration and percentage of spikes in burst showed an increasing tendency (Fig. S4C). On the other hand, the firing rate, mean burst duration, mean ISI in burst, and percentage of spikes in burst of LC neurons showed a tendency to decrease (Fig. S4D).

3.4. *α-Synuclein in the CRN neurons projected to LC and SNpc*

CRN was the early lesion site in our SNCA-stomach model and the serotonergic neurons in CRN projected to SNpc, LC, and DR (Fig. 3A−C). To study the role of CRN in PD pathology, full-length human α-synuclein tagged by EGFP (SNCA-EGFP) was overexpressed in CRN. The EGFP was used as the negative control (Fig. 3D). To investigate time-dependent effects, mice were consecutively sacrificed at 3, 9, 14, and 26 weeks. Double immunofluorescence staining against tryptophan hydroxylase (TPH) and α-synuclein indicated that α-synuclein was overexpressed in serotonergic neurons of CRN (Fig. 3E). More importantly, CRN α-synuclein projected to LC and SNpc through an anterograde axonal manner. It is worth noticing that the axonal spread of α-synuclein was increased over time, especially in SNpc (Fig. 3F).

3.5. *CRN α-synuclein led to progressive neurodegenerative changes*

To investigate the pathology induced by CRN α-synuclein, neurons in CRN, LC, and SNpc were assessed with unbiased stereological quantification. The TPH-positive neurons in CRN of SNCA-EGFP-CRN mice decreased progressively, with 29.97 ± 3.15% neuron loss at 3 weeks, 49.45 ± 1.22% at 9 weeks, 50.74 ± 3.67% at 14 weeks, and 58.44 ± 1.04% at 26 weeks post-injection (Fig. 4A and D). It is worth noticing that progressive axonotmesis and cell body shrinkage were observed in SNCA-EGFP-CRN mice at 9, 14, and 26 weeks (Fig. 4G). Similar neurodegeneration was found in LC with 22.44 ± 1.84% neuron loss at 9 weeks, 39.68 ± 5.61% at 14 weeks, and 43.13 ± 2.84% at 26 weeks (Fig. 4B and E). Also, in SNpc, significant neuron loss was observed with 24.24 ± 3.79% at 9 weeks, 41.83 ± 2.50% at 14 weeks, and 51.33 ± 3.02% at 26 weeks (Fig. 4C and F). Furthermore, the TH-positive fibers in the striatum of SNCA-EGFP-CRN mice decreased at 9, 14, and 26 weeks post-injection compared to those of EGFP-CRN mice (Fig. 4H and I). Overall, our data reveal that overexpressed α-synuclein in CRN induced progressive neurodegeneration not only in the CRN *in situ* but also in LC and SNpc *via* axonal terminals.

3.6. *CRN α-synuclein led to phosphorylated and aggregated α-synuclein accumulation*

PD pathogenesis is characterized by the accumulation of aggregates and phosphorylated α-synuclein[28]. Accumulation of α-synuclein aggregates was observed in CRN of

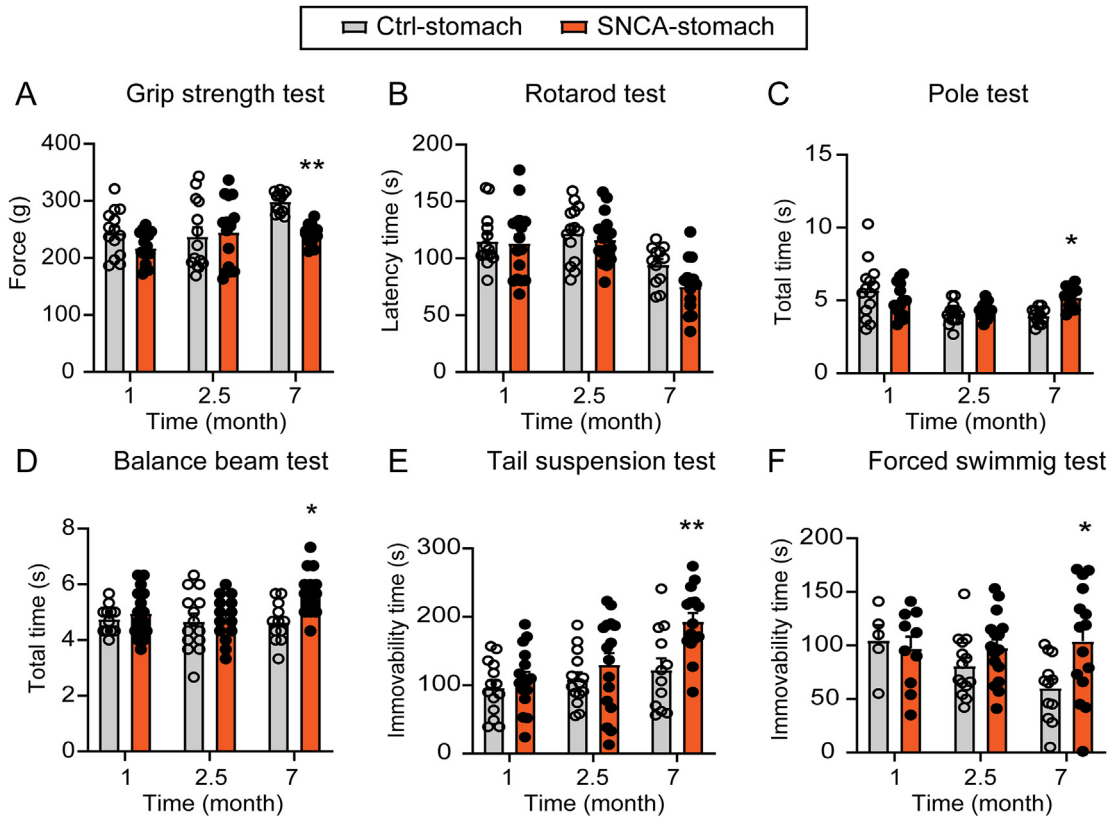

Figure 2 Gastric α-synuclein induced PD-like behavior. (A−D) Behavioral tests for motor deficits in SNCA-stomach model. Grip strength test (A). Rotarod test (B). Pole test (C). Balance beam test (D). (E, F) Behavioral tests for depression in SNCA-stomach model. Tail suspension test (E). Forced swimming test (F). Values are presented as mean ± SEM, $n = 8-16$. Two-way ANOVA followed by Tukey's or Sidak's *post hoc* test, $^{*}P < 0.05$, $^{**}P < 0.01$ *versus* Ctrl-stomach group.

SNCA-EGFP-CRN mice at 3 weeks post-injection and increased with time. The aggregates first displayed homogeneous staining, then became a refined structure with a dense core and peripheral fibrillar surroundings at 14 and 26 weeks post-injection (Fig. 5A and E), indicating mature aggregates were formed[29]. At 26 weeks post-injection, the total α-synuclein in the brainstem and midbrain was significantly increased in SNCA-EGFP-CRN mice, with no obvious signal detected in the striatum and the EGFP-CRN group (Supporting Information Fig. S5A and S5B).

Then, we assessed the level of phosphorylated α-synuclein (p-α-synuclein). We found that p-α-synuclein progressively accumulated in the CRN of SNCA-EGFP-CRN mice and projected to LC and SNpc along axons (Fig. 5B−D, F). The p-α-synuclein level in the brainstem was higher than that in the midbrain, no obvious signals were found in the striatum and the EGFP-CRN mice (Fig. S5C and S5D). It's worth mentioning that p-α-synuclein exhibited a dense core surrounded by radiating filaments at 14 weeks (Fig. 5B). Interestingly, the p-α-synuclein contained axons in LC were mainly displayed as consecutive dots, while in the SNpc, there were more labeled fibers. Lewy neurites were formed in LC and SNpc at 14 weeks in SNCA-EGFP-CRN mice, especially in SNpc (Fig. 5C and D). Moreover, there was an increase in gastric α-synuclein in SNCA-EGFP-CRN mice (Fig. S5E and S5F). These results reveal that CRN α-synuclein also affected the α-synuclein homeostasis in the gastrointestinal tract.

3.7. CRN α-synuclein led to PK-resistance α-synuclein and Lewy body formation

The formation of the Lewy body was the key to inducing neurodegeneration[30]. Sections were pretreated with proteinase K (PK) to assess the level of insoluble protein. PK-resistance α-synuclein was observed at 3 weeks post-injection in CRN of SNCA-EGFP-CRN mice, and mature structures were found at 14 weeks (Fig. 5G). The insoluble α-synuclein formation was consistent with the development of α-synuclein aggregates and p-α-synuclein. Interestingly, insoluble α-synuclein fibers formed at 3 weeks in SNpc, but not in LC at this time point. More importantly, Lewy neurite was found at 14 weeks in SNpc (Fig. 5H and I). However, insoluble α-synuclein positive inclusions were observed in the cell body in LC at 26 weeks, indicating the formation of Lewy bodies in LC neurons (Fig. 5H). No PK-resistance α-synuclein was found in EGFP-CRN mice. Together, these results demonstrated that Lewy body pathology was formed at 9 weeks in CRN, LC, and SNpc, and matured at 14 weeks, and SNpc was more vulnerable to α-synuclein pathology.

Double immunofluorescence staining against α-synuclein and ubiquitin was used to further confirm the Lewy body pathology[31]. Co-localization of α-synuclein and ubiquitin was found in CRN at 3 weeks of SNCA-EGFP-CRN mice (Fig. 5J). On the other hand, the p62-positive cell was rare at 3 weeks and increased in the SNCA-EGFP-CRN mice.

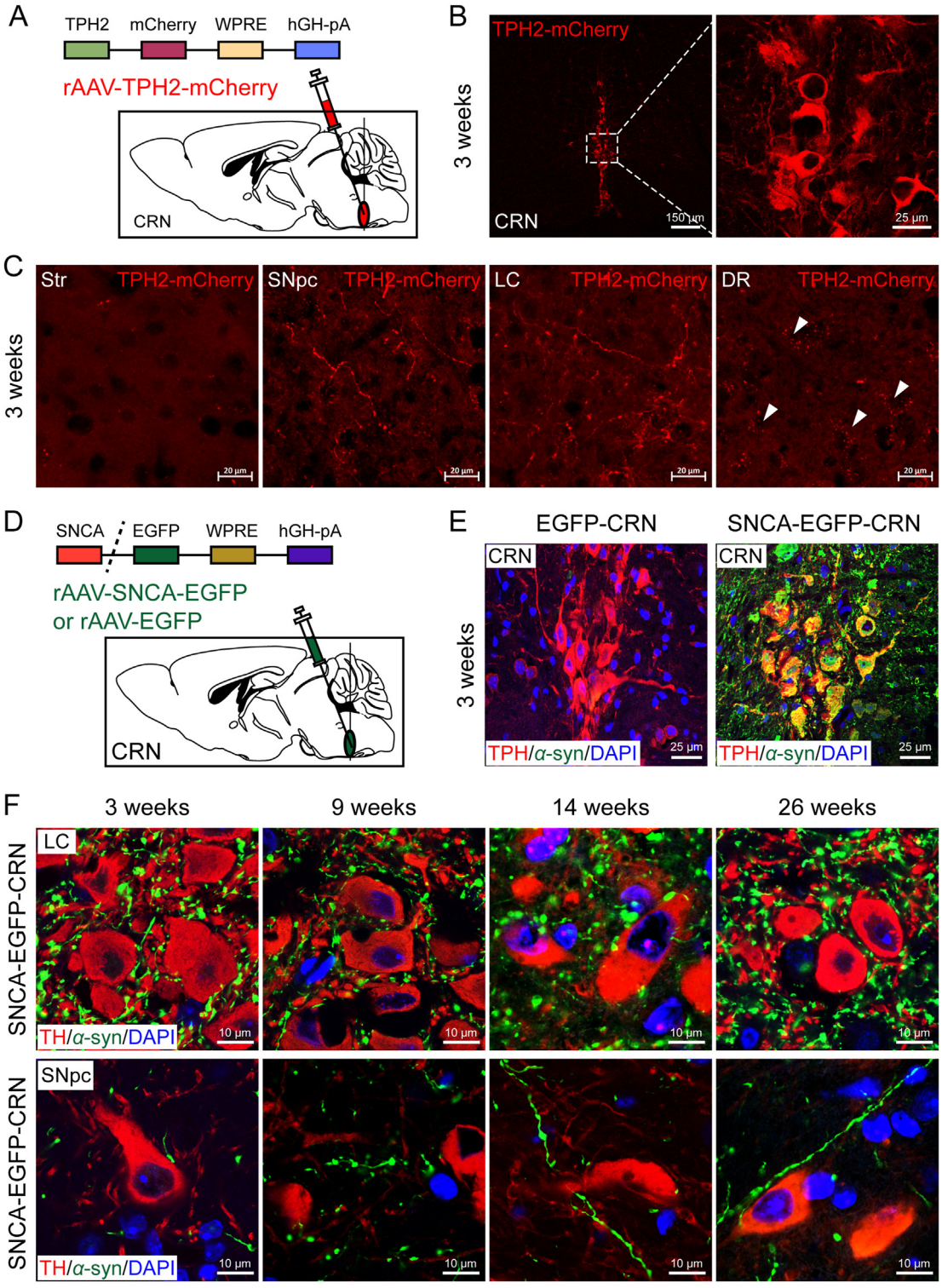

Figure 3 Axonal projection of serotonergic neurons and CRN α-synuclein. (A, B) rAAV-TPH2-mCherry vector expression in the serotoninergic neurons in CRN at 3 weeks post-injection. Scale bar: 150 or 25 μm. (C) Serotoninergic neurons in CRN projected to SNpc, LC, and DR at 3 weeks post-injection. Scale bar: 20 μm. (D, E) rAAV-SNCA-EGFP or rAAV-EGFP vector expression in CRN. Scale bar: 25 μm. (F) The overexpressed α-synuclein in CRN projected to LC and SNpc along axons at 3, 9, 14, and 26 weeks. Scale bar: 10 μm. $n = 3$. Abbreviations: caudal raphe nuclei (CRN), locus coeruleus (LC), substantia nigra pars compacta (SNpc), dorsal raphe nuclei (DR).

Co-localization of α-synuclein and p62 was observed at 14 and 26 weeks (Fig. 5K), indicating that Lewy bodies were formed. Taken together, our data reveal that ubiquitin-positive inclusions were formed at 3 weeks, and p62-positive inclusions were formed later. These results were consistent with the immunohistochemistry staining.

3.8. CRN α-synuclein led to neuroinflammation

Neuroinflammation is closely associated with the neurodegeneration process[32,33]. To investigate the neuroinflammation induced by CRN α-synuclein, we detected the amount and state of microglia and astrocytes in CRN, LC, and SNpc, where the neuron loss was significant. Microglia increased in the CRN, LC, and SNpc at 14 and 26 weeks post-injection of SNCA-EGFP-CRN mice compared to EGFP-CRN mice, with increased process complexity and enlarged cell bodies (Supporting Information Fig. S6A, S6B, S6E), indicating microglia activation. Similarly, the increased astrocytes with enlarged cell bodies, process thickening, and elongation were also found in the same brain regions of SNCA-EGFP-CRN mice at 14 and 26 weeks (Fig. S6C, S6D, S6F), indicating astrogliosis and activation. Increased TNF-α was observed as well in the SNCA-EGFP-CRN mice (Fig. S6G and S6H). Interestingly, the SNCA-EGFP-CRN mice showed activated astrocyte captured the α-synuclein with the elongated process in CRN (Supporting Information Fig. S7). Taken together, these results show that CRN α-synuclein promoted neuroinflammation in CRN, LC, and SNpc.

3.9. CRN α-synuclein led to progressive motor deficits and depressive-like symptoms

To assess the motor function of the CRN model, pole test, rotarod test, grip strength test, and balance beam test were used. The SNCA-EGFP-CRN mice showed a significant decrease in the grip strength and latency time in the rotarod test compared to EGFP-CRN mice at 9, 14, and 26 weeks post-injection (Fig. 6A and B). The time in the pole test was increased in all the time points in the SNCA-EGFP-CRN mice (Fig. 6C, Supporting Information Video S1). The time spent in the balance beam test increased significantly at 9, 14, and 26 weeks as well (Fig. 6D, Supporting Information Video S2). More importantly, the SNCA-EGFP-CRN mice showed more significant differences compared to the EGFP-CRN group at 14 and 26 weeks (Fig. 6B−D), indicating progressive motor dysfunction. Taken together, the SNCA-EGFP-CRN mice exhibited progressive strength loss and motor deficits.

The forced swimming test and tail suspension test were used for depressive-like symptoms. SNCA-EGFP-CRN mice showed increased immobility time in the tail suspension test at 14 and 26 weeks post-injection. A similar tendency was observed in the forced swimming test (Fig. 6E and F). These results demonstrate that CRN α-synuclein led to depression-like disorder.

Supplementary video related to this article can be found at https://doi.org/10.1016/j.apsb.2024.01.015

We also used the open field test and elevated plus test to assess anxiety-like behaviors, and the Y-maze test and novel object recognition test to investigate memory deficits. During the open field test, the center entries significantly decreased in the SNCA-EGFP-CRN mice compared to EGFP-CRN mice at 26 weeks post-injection (Fig. 6G and H). However, no statistical difference was found in the elevated plus-maze test (Fig. 6I and J). These results suggest that the anxiety-like symptoms induced by overexpressed α-synuclein were mild. Furthermore, there was no difference in the Y maze test and novel object recognition test (Fig. 6K−N), suggesting no memory loss until 26 weeks post-injection.

3.10. CRN α-synuclein led to disordered firing activities of LC and SNpc neurons

To investigate the neuronal firing activity changes induced by CRN α-synuclein, the neuron firing activity in LC and SNpc was detected under movement and anesthesia (Supporting Information Tables S2 and S3). Power spectral density (PSD) was used to assess the local field potential (LFP). Firing activity was assessed by firing rate and firing pattern [mean burst duration, interspike interval (ISI), and percentage of spikes in burst].

During movement, the dopaminergic neurons in SNpc of SNCA-EGFP-CRN mice showed decreased LFP at 4 weeks, especially under 40 Hz, and a decreased tendency in the firing rate and mean burst duration (Supporting Information Fig. S8A). At 9 weeks, an increase in LFP and a significant decrease in the firing rate and percentage of spikes in burst were found (Fig. 7A). At 14 weeks, the LFP increased while no significant changes were found in the firing rate and patterns in SNpc neurons (Fig. S8B). At 26 weeks, increased LFP and decreased ISI were detected in dopaminergic neurons of SNCA-EGFP-CRN mice (Fig. 7B). Similarly, during movement, the LC neurons showed no significant changes in the firing activity at 4 weeks of SNCA-EGFP-CRN mice (Fig. S8C). At 9 weeks, significantly increased LFP and firing rate of LC neurons were found (Fig. 7C). At 14 weeks, increased LFP, firing rate and mean burst duration were detected in the SNCA-EGFP-CRN mice (Fig. S8D). At 26 weeks, on the contrary, the firing rate, mean burst duration and percentage of spikes in burst decreased significantly (Fig. 7D).

Under anesthesia, the activities of SNpc neurons in SNCA-EGFP-CRN mice showed decreased LFP and no significant changes compared to EGFP-CRN mice at 4 weeks (Supporting Information Fig. S9A). At 9 and 14 weeks, the LFP was increased under 40 Hz (Fig. 8A, Fig. S9B). However, at 26 weeks, SNCA-EGFP-CRN mice showed a significant increase in the firing rate, mean burst duration, and mean ISI in burst of SNpc neurons under anesthesia compared to EGFP-CRN mice (Fig. 8B). On the other hand, the LC neurons in the SNCA-EGFP-CRN mice showed decreased mean burst duration, ISI and percentage of spikes in the burst at 4 weeks (Fig. S9C). At 9 and 14 weeks, the increased firing rate, mean burst duration and percentage of spikes were found (Fig. 8C, Fig. S9D). However, at 26 weeks post-injection, only a decrease tendency of firing rate, mean burst duration and percentage of spikes in burst was observed in LC neurons of SNCA-EGFP-CRN mice (Fig. 8D).

3.11. Dorsal RN did not further spread α-synuclein to LC and SNpc

The dorsal raphe nucleus (DR) consists of most serotonergic neurons and is located in the rostral RN in the midbrain. The CRN α-synuclein was also projected to DR in SNCA-EGFP-CRN mice (Supporting Information Fig. S10A). And the p-α-synuclein and insoluble forms were increased in DR (Fig. S10B and S10C). However, the TPH-positive cells in DR were not damaged until 26 weeks (Fig. S10D and S10E). The serotonergic neurons in DR were not projected into CRN, LC, SNpc, and striatum (Fig. S10F−S10H). These results indicate that serotoninergic neurons in DR were not susceptible to α-synuclein compared to neurons in CRN, LC, and SNpc. Although α-synuclein spread along the axons to the DR region, serotonergic neurons in DR may not continue to propagate α-synuclein further to the LC and SNpc.

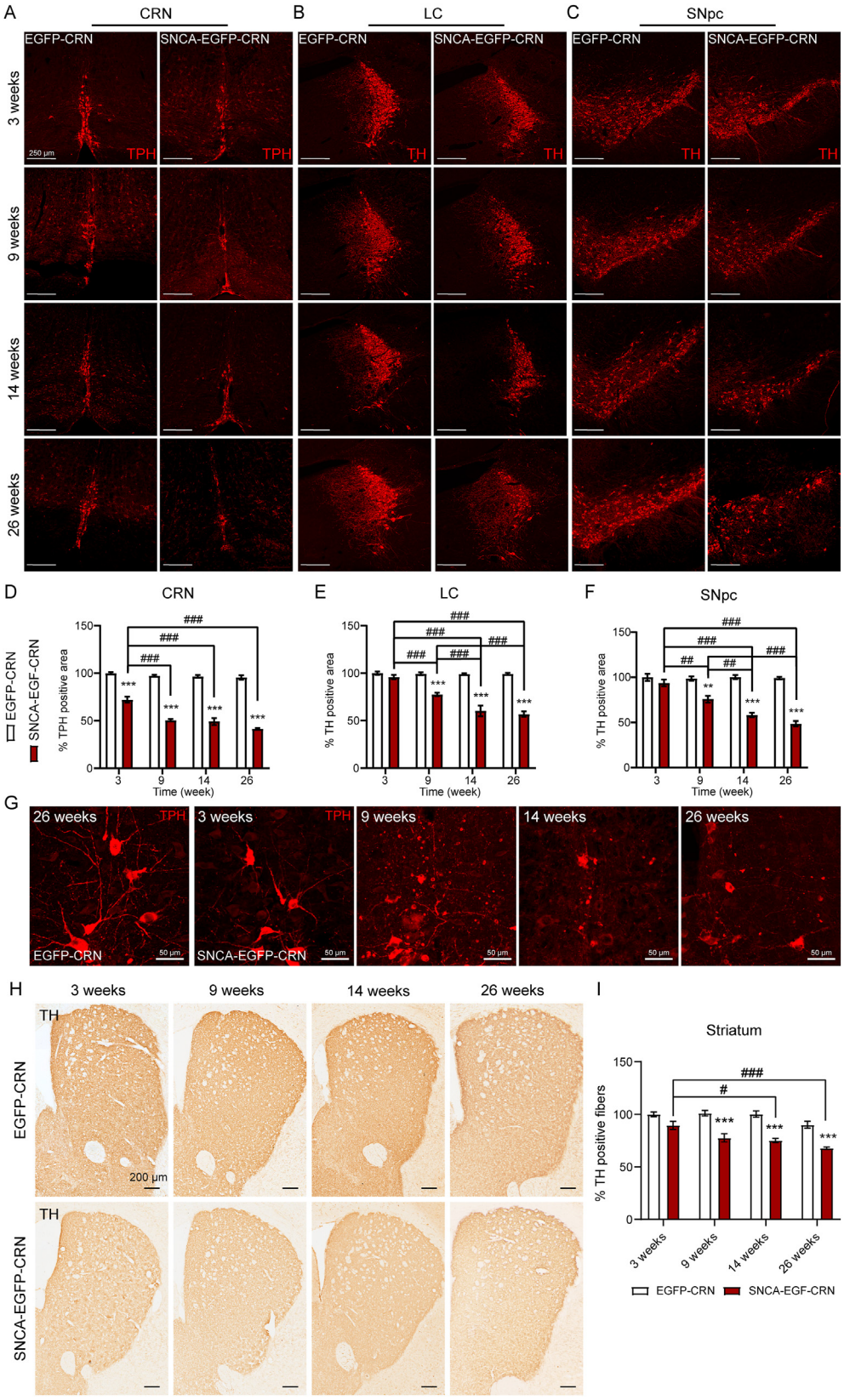

Figure 4 Progressive neuron loss induced by overexpressed α-synuclein in the CRN. (A) Representative images of TPH-positive neurons in CRN at 3 weeks, 9 weeks, 14 weeks, and 26 weeks. Scale bar: 250 μm. (B) Representative images of TH-positive neurons in LC at 3 weeks, 9, 14, and 26 weeks. Scale bar: 250 μm. (C) Representative images of TH-positive neurons in SNpc at 3, 9, 14, and 26 weeks. Scale bar: 250 μm. (D) The quantification of TPH-positive neurons in CRN. (E) The quantification of TH-positive neurons in LC. (F) The quantification of TH-positive neurons in SNpc. (G) Representative images of the TPH-positive cell body pyknosis and axonal disruption in CRN at 9, 14, and 26

4. Discussions

The major findings of this study provide evidence that CRN acts as the hub linking the gastrointestinal tract and midbrain. CRN is the early lesion site of gastric α-synuclein and CRN α-synuclein could further induce Lewy body pathology and PD-like behavior (Fig. 9). Single photon emission computed tomography (SPECT) studies have shown that the raphe serotonin transporter availability in the brainstem of PD patients is reduced at early stage[12,13], and combing with this work, we report that CRN damage is an early event in PD progression. Our study provides valuable details to the "gut−brain" hypothesis and links it with Braak stages, and CRN might be a hallmark to predict the progression of PD.

Based on our research, we suggest that the SNCA-stomach model might be a valuable model for PD intervention at an early stage, which is earlier than that of other conventional models targeted at the midbrain. Due to the lack of underlying mechanisms in the prodromal and early PD stages, the useful model that can mimic the chronically developed pathology at the early stage is limited. The SNCA-stomach model shows neuron loss at 2.5 months while no significant motor symptoms are developed. This may be due to the compensatory mechanisms and obscure correlation between motor dysfunction and neuron loss at early stage[34,35]. Significant but less severe motor deficits are developed in the SNCA-stomach model at 7 months, along with increased neuronal firing activity. And the disturbed firing activity further contributes to the motor deficits[36]. This behavioral dysfunction is consistent with the subtle motor dysfunction in PD patients at the early stage[37]. Investigations for the long-term development of the SNCA-stomach model at a late stage are ongoing.

In the SNCA-stomach model, we report gastric α-synuclein may propagate through the spinal cord and damage CRN neurons. The CRN α-synuclein further projects to LC and SNpc and leads to progressive neuron loss. The difference in the neuron loss between SNCA-stomach and CRN models may be due to the amount of pathological α-synuclein[38]. The level of pathological α-synuclein in LC and SNpc of the SNCA-stomach model is lower than that in the SNCA-EGFP-CRN model due to the long-propagation. The SNCA-EGFP-CRN model may consequently display more direct lesions than the SNCA-stomach model. The α-synuclein accumulation in the spinal cord of the SNCA-EGFP-CRN model may be due to connections between the myenteric nerve plexus and the spinal cord[21]. Postmortem study of PD patients shows that pathological α-synuclein accumulated in the spinal cord and spread retrogradely through the preganglionic sympathetic nerves[27]. And α-synuclein overexpressed in the sciatic nerve spread along the ventral motor neurons in the spinal cord[39]. Interestingly, CRN α-synuclein propagates downward along the serotoninergic neuron axons in the spinal cord at the late time point in the SNCA-EGFP-CRN model (unpublished data). Other studies also showed increased serotonergic neurons in the spinal cord after injury[40,41]. Spinal cord damage further induces gastrointestinal dysfunction[42]. These results emphasize the potential role of the spinal cord in the bidirectional regulation.

Besides the spinal cord, the gastrointestinal α-synuclein may propagate to the brain through the vagus nerve, enteric cells, and general circulation[7,43,44] (Supporting Information Fig. S11). Research demonstrates that the vagus nerve is an important pathway for gastrointestinal α-synuclein propagating to the brain. And vagotomy helps to block the upward propagation of pathological gastrointestinal α-synuclein[7]. However, vagotomy in patients does not reduce the risk of developing PD[45]. The various neurons in the enteric nervous system and complex neuron connections may participate in the propagation of α-synuclein as well[46]. Moreover, recent research shows enteric Lewy body-induced PD pathology without vagus nerve lesions and proposes general circulation as the propagation pathway[43]. The difference in propagation manner shown in research may be due to the anatomical neural connections and characteristics of pathological seeds[47]. The general gut−brain axis involves the afferent pathways to the brain *via* spinal and vagal, and efferent signals to the gastrointestinal tract through sympathetic and parasympathetic neurons[48]. The gut of mice receives vagal afferents intervention, and the stomach receives input regulation from the spinal cord and CRN[49−51]. In addition, it is reported that the asparagine endopeptidase (AEP) mediates the fibrillization and retrograde propagation of α-synuclein from the gut to the brain, triggering dopaminergic neuronal loss and motor dysfunction[52]. The Leucine-rich repeat kinase 2 (LRRK2) G2019S mutation also facilitates the aggregation of endogenous α-synuclein in dopaminergic neurons[53]. Further investigation may focus on the complex pathways[54] and factors that participated in the propagation of gastrointestinal α-synuclein.

In this study, we highlight the essential early role of serotonergic neurons in CRN in PD pathology. CRN serotonin may be a potential biomarker for the early diagnosis of PD. Significantly lower serotonin transporter availability in the raphe nuclei is found in patients with early PD. Also, the brainstem serotonin system participates in sleep disturbances, which is an early event in PD[55,56]. The loss of the serotonin transporter increases the severity of motor symptoms[12,57]. Furthermore, the low serotonin positively correlated with high iron[58], which may further exacerbate oxidative stress and susceptibility in SNpc dopaminergic neurons. Therefore, drugs maintaining the homeostasis of CRN serotonergic neurons may help to preserve dopaminergic neurons in SNpc. We also observe the increased α-synuclein in the stomach induced by CRN α-synuclein overexpression, further forming a vicious cycle. This result may be due to the descending regulation of the CRN to the stomach through the vagus verve and spinal cord[40,59].

In addition to CRN, DR is also part of RN and secretes most of the serotonin[11]. Research suggests that DR is related to the development of tremors and depression in PD patients[60]. However, overexpressing α-synuclein in DR fails to induce behavioral impairment[61]. Our results show that DR receives the α-synuclein positive axonal projections from CRN, but may not further propagate α-synuclein to other regions. Taken together, these findings suggest that although DR is the major nucleus secreting serotonin, lesions in the CRN exhibit a more direct PD pathogenicity.

In our study, multiple staining results for α-synuclein pathological markers confirm the progressive Lewy body pathology

weeks. Scale bar: 50 μm. (H) Representative images of TH-positive fibers in the striatum at 3, 9, 14, and 26 weeks. Scale bar: 200 μm. (I) The quantification of TH-positive fibers in the striatum. Values are presented as mean ± SEM, EGFP-CRN at 3 weeks was set as 100%, $n = 3$. Two-way ANOVA followed by multiple comparison, $^{\#}P < 0.05$, $^{\#\#}P < 0.01$, $^{\#\#\#}P < 0.001$ *versus* SNCA-EGFP-CRN group; $^{**}P < 0.01$, $^{***}P < 0.001$ *versus* EGFP-CRN group. Abbreviations: caudal raphe nuclei (CRN), locus coeruleus (LC), substantia nigra pars compacta (SNpc).

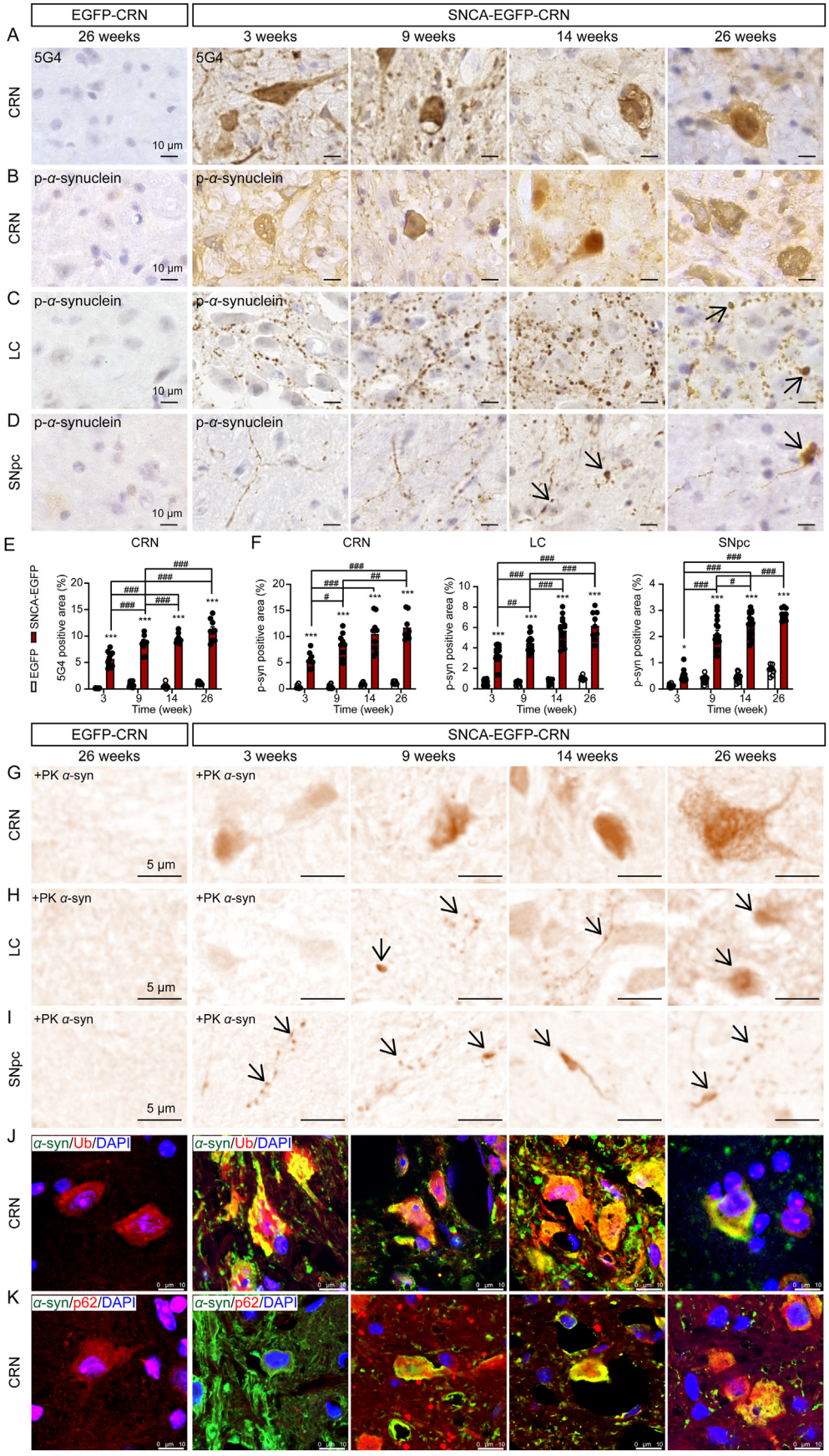
EGFP-CRN
SNCA-EGFP-CRN
A
26 weeks
3 weeks
9 weeks
14 weeks
26 weeks
CRN
5G4
10 μm
B
p-α-synuclein
CRN
C
LC
D
SNpc
E
CRN
F
CRN
LC
SNpc
EGFP
SNCA-EGFP
5G4 positive area (%)
p-syn positive area (%)
Time (week)
G
+PK α-syn
5 μm
H
I
J
α-syn/Ub/DAPI
K
α-syn/p62/DAPI

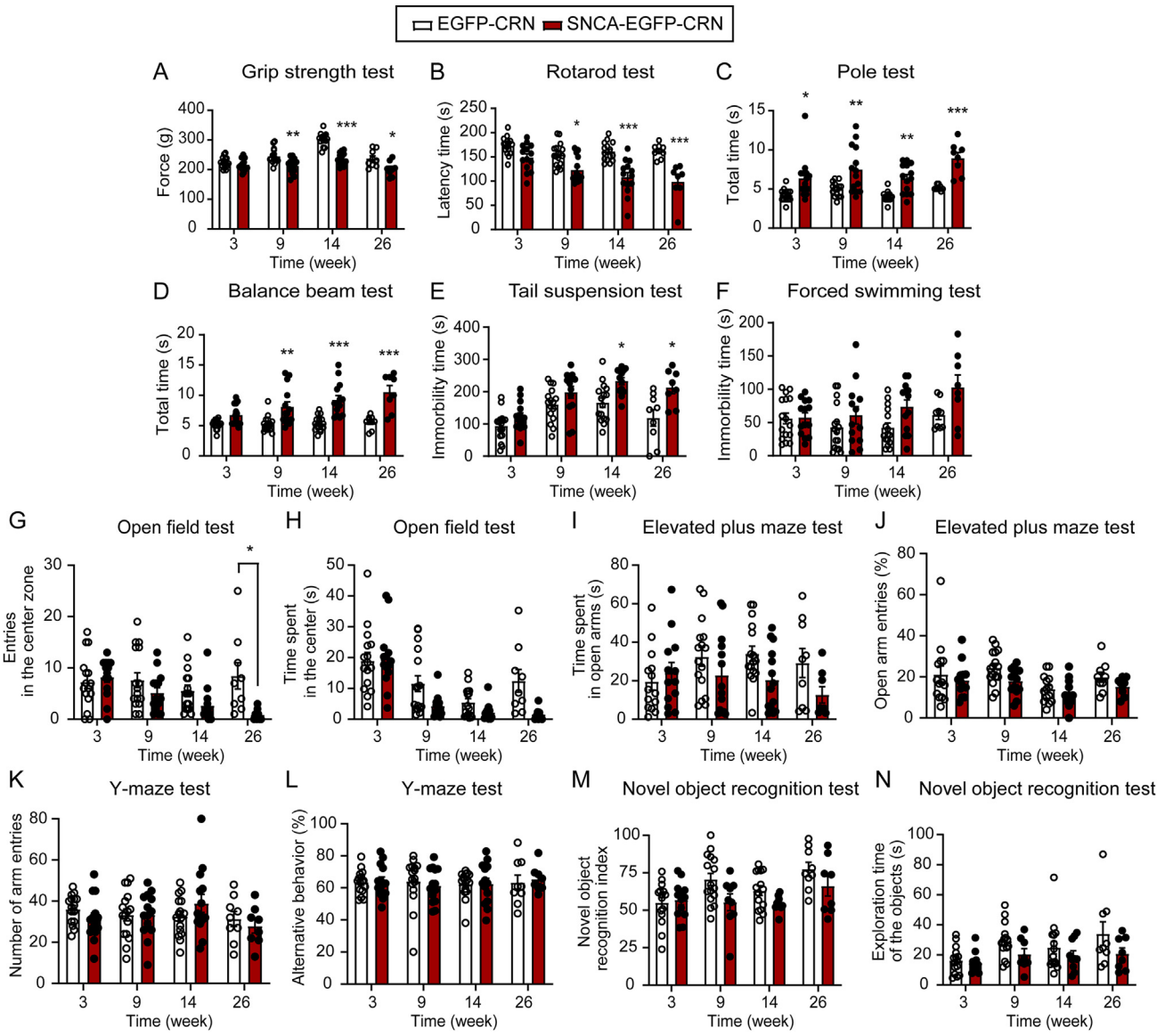

Figure 6 CRN α-synuclein induced motor and non-motor symptoms over 26 weeks. (A−D) Behavioral tests for motor deficits in SNCA-EGFP-CRN model. Grip strength test (A). Rotarod test (B). Pole test (C). Balance beam test (D). (E−N) Behavioral tests for non-motor deficits in SNCA-EGFP-CRN model. Tail suspension test (E). Forced swimming test, although the SNCA-EGFP-CRN group showed a tendency to increase immobility time, there were no significant differences compared to the EGFP-CRN group (F). Open field test (G, H). Elevated plus maze test (I, J). Y-maze test (K, L). Novel object recognition test (M, N). Values are presented as mean ± SEM. $n = 14$−16. Two-way ANOVA followed by Tukey's or Sidak's *post hoc* test, $^{*}P < 0.05$, $^{**}P < 0.01$, $^{***}P < 0.001$ *versus* EGFP-CRN group.

caused by CRN α-synuclein. More importantly, the time of formation and maturity of the Lewy body is consistent with the development of motor symptoms and depression. At 9 weeks, both Lewy body pathology and significant dyskinesia are observed. And mature Lewy bodies are formed in CRN at 14 weeks, while depressive behavior is present at the same time point. Taken

Figure 5 Overexpressing α-synuclein in CRN led to progressive Lewy body pathology. (A) The immunochemistry staining of α-synuclein aggregates (stained by antibody 5G4) in CRN at 3, 9, 14, and 26 weeks post-injection. Scale bar: 10 μm. (B−D) Representative images of p-α-synuclein in CRN (B), LC (C), and SNpc (D) at 3, 9, 14, and 26 weeks post-injection. Scale bar: 10 μm. (E) Quantification of α-synuclein aggregates in CRN at 3, 9, 14, and 26 weeks post-injection. (F) Quantification of p-α-synuclein in CRN, LC and SNpc at 3, 9, 14, and 26 weeks post-injection. (G−I) Accumulation of insoluble α-synuclein in CRN (G), LC (H), and SNpc (I) at 3, 9, 14, and 26 weeks post-injection. Scale bar: 5 μm. (J) Double immunostaining against ubiquitin and α-synuclein in CRN at 3, 9, 14, and 26 weeks post-injection. Scale bar: 10 μm. (K) Double immunostaining against p62 and α-synuclein in CRN at 3, 9, 14, and 26 weeks post-injection. Scale bar: 10 μm. Values are presented as mean ± SEM, $n = 3$. Two-way ANOVA followed by Tukey's *post hoc* test, $^{*}P < 0.05$, $^{***}P < 0.001$ *versus* EGFP-CRN group; $^{\#}P < 0.05$, $^{\#\#}P < 0.01$, $^{\#\#\#}P < 0.001$ *versus* SNCA-EGFP-CRN group. Abbreviations: caudal raphe nuclei (CRN), locus coeruleus (LC), substantia nigra pars compacta (SNpc).

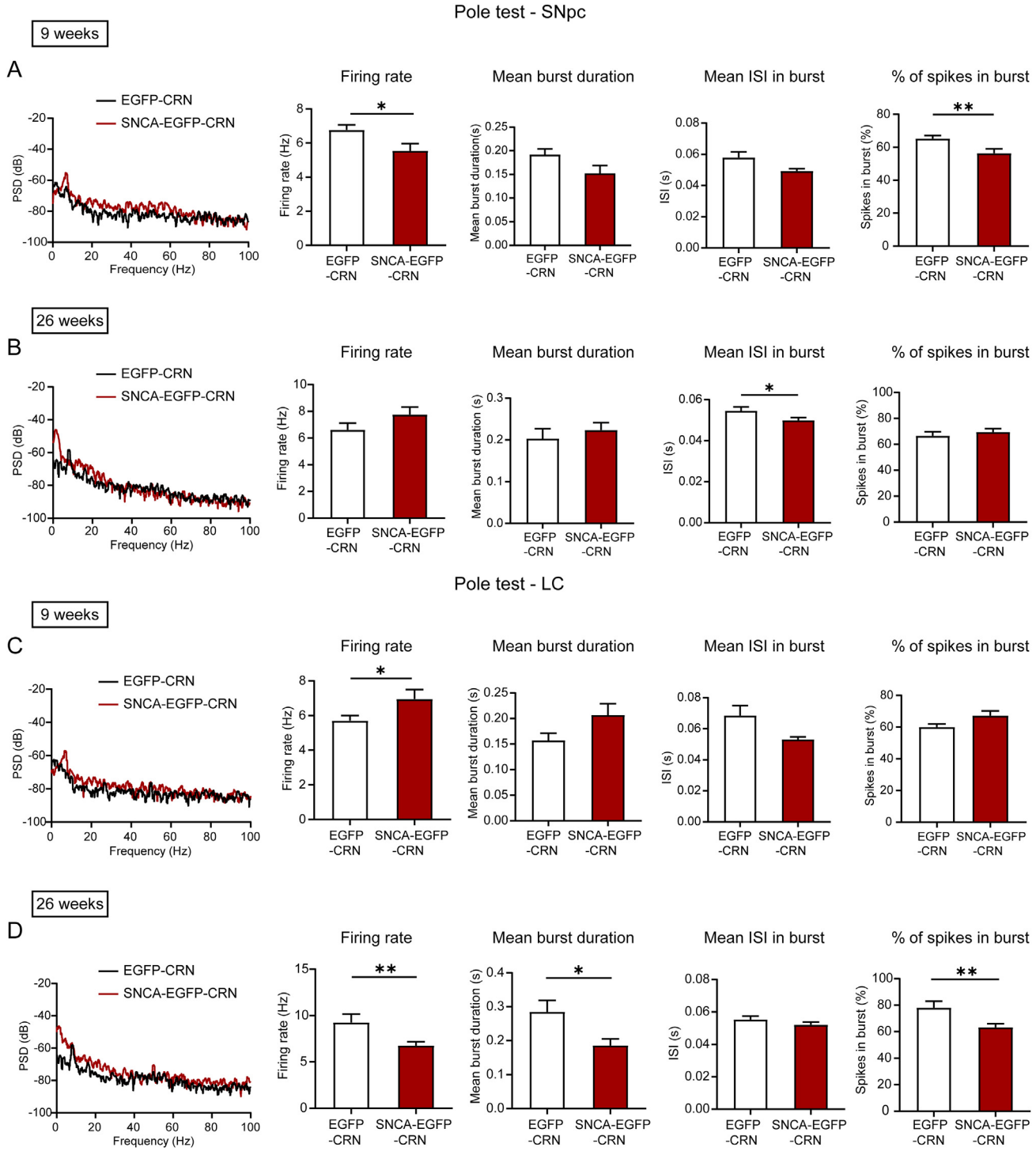

Figure 7 The abnormal local field potential and neuron firing activity in SNpc and LC in motion induced by CRN α-synuclein overexpression. (A, B) The statistics of power spectral density (PSD), firing rate, and firing pattern in SNpc neurons at 9 weeks (A) and 26 weeks (B) post-injection during mice climbing down the pole. (C, D) The statistics of PSD, firing rate, and firing pattern in LC neurons at 9 weeks (C) and 26 weeks (D) during pole test. Values are presented as mean ± SEM. $n = 3-4$. Statistical significance was determined using two-tailed Student's *t*-test, $^{*}P < 0.05$, $^{**}P < 0.01$. Abbreviations: interspike interval (ISI), locus coeruleus (LC), substantia nigra pars compacta (SNpc).

together, our results show a precise time point of the formation and propagation of Lewy pathology and link it with the behavioral symptoms. Reducing pathological α-synuclein neuron-to-neuron transfer might slow the disease progression[62–65]. The CRN α-synuclein projection patterns are also different. Swollen and distorted insoluble α-synuclein positive axons are observed in SNpc at 3 weeks, which is earlier than those in LC. Increased α-synuclein interferes with the normal synaptic function and

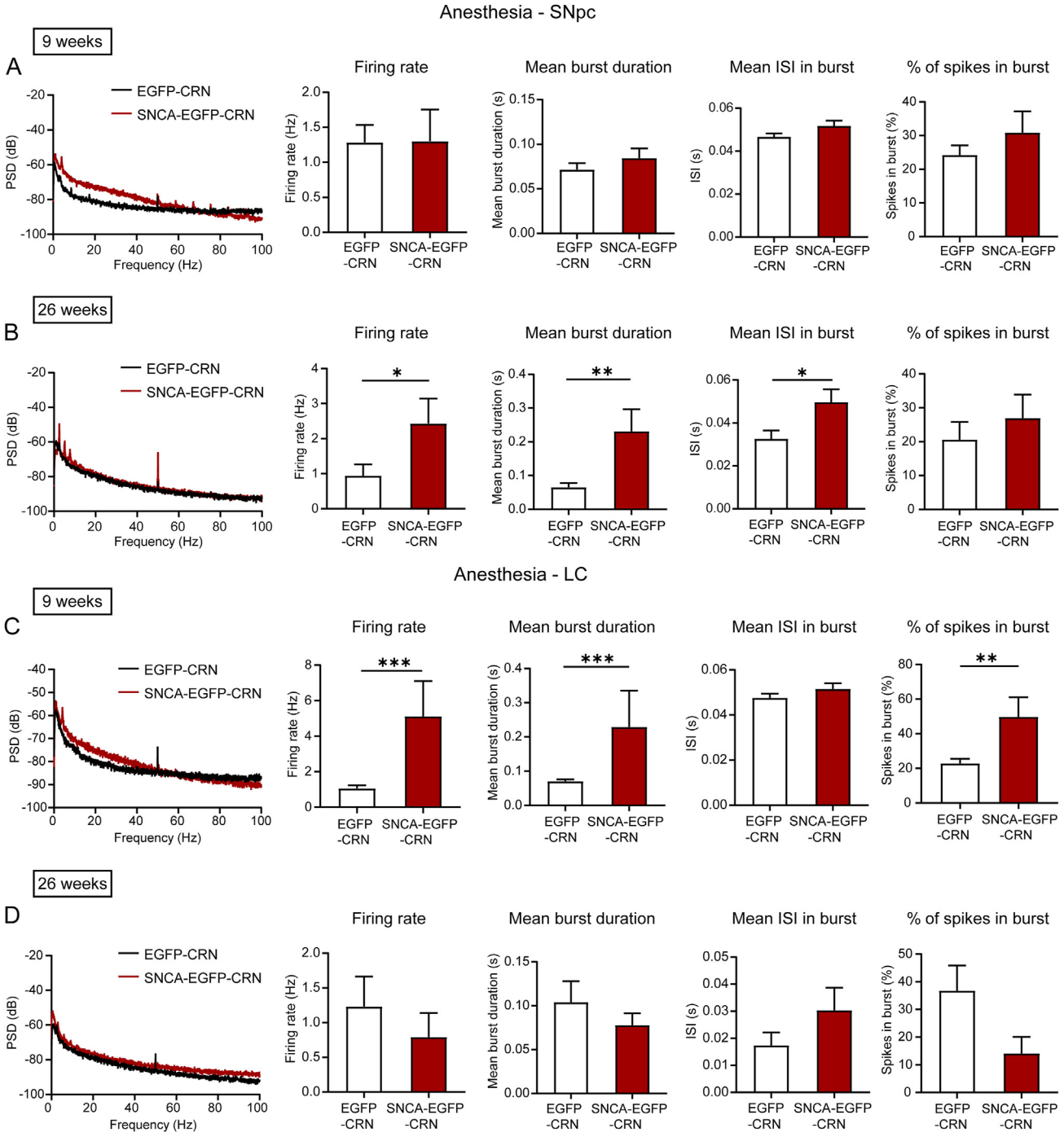

Figure 8 The abnormal local field potential and neuron firing activity in SNpc and LC under anesthesia induced by CRN α-synuclein overexpression. (A, B) The statistics of power spectral density (PSD), firing rate, and firing pattern in SNpc neurons at 9 weeks (A) and 26 weeks (B) post-injection under anesthesia. (C, D) The statistics of PSD, firing rate, and firing pattern in LC neurons at 9 weeks (C) and 26 weeks (D) under anesthesia. Values are presented as mean ± SEM, $n = 3-4$. Statistical significance was determined using two-tailed Student's *t*-test, $^{*}P < 0.05$, $^{**}P < 0.01$, $^{***}P < 0.001$. Abbreviations: interspike interval (ISI), locus coeruleus (LC), substantia nigra pars compacta (SNpc).

inter-organelle contacts[66]. Varicosity and axonal transport defects promote the degeneration of dopaminergic neurons[67,68].

Similar electrophysiology changes are observed in the CRN model (6 months) and the stomach model (7 months), further suggesting that CRN is the hub between the stomach and the midbrain. However, the spikes of LC neurons increase during the pole test in the SNCA-stomach model at 7 months, while the activity decreases in the SNCA-EGFP-CRN model at 26 weeks. This may be because the gastric α-synuclein may also travel to the brain in multiple ways and influence LC neuron activity[7,69,70]. The firing dysfunction of SNpc and LC neurons relates to neuron loss and motor and non-motor symptoms. In this work, we show increased LFP and changed neuron firing activities of SNpc and LC neurons. The increasing LFP indicates exaggerated oscillatory

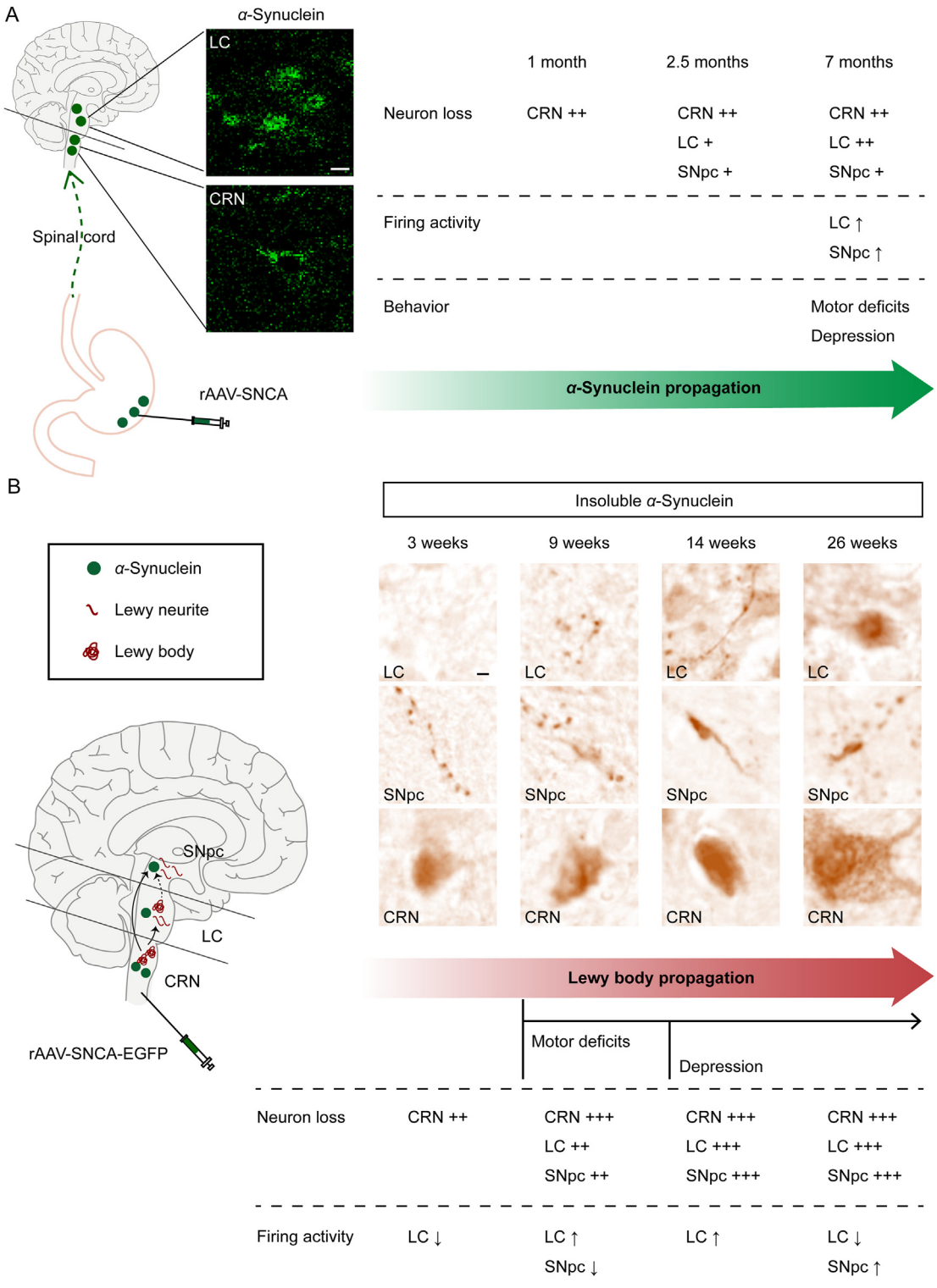

Figure 9 Graphic summary of gastric and CRN α-synuclein pathology. (A) The graphic summary of overexpressed α-synuclein in the stomach propagation to CRN and LC. Gastric α-synuclein leads to neuron loss and motor and non-motor deficits over a time frame of 7 months. Scale bar: 10 μm. (B) The graphic summary of overexpressed α-synuclein in CRN propagation to LC and SNpc. The overexpressed α-synuclein in CRN leads to progressive Lewy body pathology, neuron loss, neuron firing dysfunction, and motor and non-motor deficits. The representative images are captured from the typical results of immunochemistry staining in Fig. 5. Scale bar: 1 μm "+" represents neuron loss under 20%. "++" represents neuron loss between 20% and 30%. "+++" represents neuron loss between 30% and 50%. "↑" represents increased neuron firing rate and activity. "↓" represents decreased neuron firing rate and activity. Abbreviations: caudal raphe nuclei (CRN), locus coeruleus (LC), substantia nigra pars compacta (SNpc).

synchrony and is correlated with the severity of rigidity and tremor[71,72]. The changed firing patterns in dopaminergic neurons are not uniformed in different models and pathological stages[73−75]. The decreased firing activity of dopaminergic neurons may be due to the mitochondrial and membrane potential dysfunction and therefore decreases the dopamine concentration, which further leads to motor impairment[36]. The increased firing rate and burst firing activity in dopaminergic neurons are accompanied by an intracellular calcium increase, which further leads to oxidative stress and neuron loss[75]. The abnormal firing activity in LC neurons also exacerbates the dopaminergic neuron pathology and participates in motor deficits, depression-like behavior, and REM sleep disturbance[76−79]. The changes in LC firing rate relate to Ca^{2+}-activated K channels dysfunction, which are involved in antioxidant and maintenance of mitochondrial function[80−82]. The detailed mechanism needs further investigation.

The firing activity dysfunction in SNpc and LC further indicates a potential neuronal circuit. The SNpc neuron firing rate decreases at early time points and does not increase until the LC neuron firing rate is significantly decreased in the SNCA-EGFP-CRN model, this may be due to the overactivation of LC neurons that inhibits the activity of SNpc neurons[83]. The noradrenergic neurons in LC directly project to SNpc and noradrenaline secreted by LC neurons regulates the dopaminergic neurons firing activity through activated D2 receptors[83,84]. The LC neuron pathology promotes the degeneration of dopaminergic neurons[76,85−87]. It is interesting that LC also receives direct regulation by serotonin[88,89]. Stimulation of serotoninergic neurons in RN reduces neuronal activity in LC and sustained serotonin promotes noradrenaline release[90,91]. On the other hand, SNpc neuronal activity changes significantly when the majority of CRN neurons are lost in the SNCA-EGFP-CRN model, this may be due to the depletion of serotonin[92]. Low echo in CRN detected by transcranial sonography connects with high echo in SNpc in idiopathic REM sleep behavior disorder[93]. Inhibiting the serotonin transporter promotes dopaminergic neuron loss[94]. Maintaining the homeostasis of CRN and LC neurons may help to reduce the venerability of dopaminergic neurons.

5. Conclusions

Our study constructed a valuable model for PD intervention at an early stage and provides detailed evidence that connects the Braak stages and the "gut−brain" axis hypothesis. We report that gastric α-synuclein pathology further propagates to LC and SNpc through serotoninergic neurons in CRN. The Lewy body pathology is transported along axons to projected brain regions, further inducing abnormal neuronal firing activity, and motor and non-motor symptoms. The formation of abnormal α-synuclein and Lewy bodies in our model is progressive and distinct. Furthermore, we provide evidence for potential neuron circuits between CRN, LC, and SNpc.

Acknowledgment

This work was supported by the Natural Science Foundation of Beijing Municipality (No. 7212156, China), CAMS Innovation Fund for Medical Sciences (CIFMS, 2021-I2M-1−026, China), National Natural Science Foundation of China, China (82373852).

Author contributions

All authors reviewed and approved the final version of the article. All authors contributed to the study conception and design. The experimental design and funding acquisition were conducted by Yuhe Yuan. The study was supervised by Nahong Chen. The experiments to express α-synuclein in the stomach and related detection were performed by Ruxue Bo and Tiantian Zhou. The experiments to express α-synuclein in the CRN and related detection were performed by Chenglu Zhang. The manuscript was written and edited by Chenglu Zhang.

Conflicts of interest

The authors have declared no conflict of interest.

Appendix A. Supporting information

Supporting data to this article can be found online at https://doi.org/10.1016/j.apsb.2024.01.015.

References

1. Dauer W, Przedborski S. Parkinson's disease: mechanisms and models. *Neuron* 2003;**39**:889−909.
2. Tysnes OB, Storstein A. Epidemiology of Parkinson's disease. *J Neural Transm* 2017;**124**:901−5.
3. Raza C, Anjum R, Shakeel NUA. Parkinson's disease: mechanisms, translational models and management strategies. *Life Sci* 2019;**226**:77−90.
4. Bloem BR, Okun MS, Klein C. Parkinson's disease. *Lancet* 2021;**397**:2284−303.
5. Braak H, Del Tredici K, Rüb U, de Vos RA, Jansen Steur EN, Braak E. Staging of brain pathology related to sporadic Parkinson's disease. *Neurobiol Aging* 2003;**24**:197−211.
6. Klingelhoefer L, Reichmann H. Pathogenesis of Parkinson disease—the gut−brain axis and environmental factors. *Nat Rev Neurol* 2015;**11**:625−36.
7. Kim S, Kwon SH, Kam TI, Panicker N, Karuppagounder SS, Lee S, et al. Transneuronal propagation of pathologic α-synuclein from the gut to the brain models Parkinson's disease. *Neuron* 2019;**103**:627−641.e7.
8. Van Den Berge N, Ferreira N, Gram H, Mikkelsen TW, Alstrup AKO, Casadei N, et al. Evidence for bidirectional and trans-synaptic parasympathetic and sympathetic propagation of α-synuclein in rats. *Acta Neuropathol* 2019;**138**:535−50.
9. Challis C, Hori A, Sampson TR, Yoo BB, Challis RC, Hamilton AM, et al. Gut-seeded α-synuclein fibrils promote gut dysfunction and brain pathology specifically in aged mice. *Nat Neurosci* 2020;**23**:327−36.
10. Hornung JP. The human raphe nuclei and the serotonergic system. *J Chem Neuroanat* 2003;**26**:331−43.
11. Jacobs BL, Azmitia EC. Structure and function of the brain serotonin system. *Physiol Rev* 1992;**72**:165−229.
12. Qamhawi Z, Towey D, Shah B, Pagano G, Seibyl J, Marek K, et al. Clinical correlates of raphe serotonergic dysfunction in early Parkinson's disease. *Brain* 2015;**138**:2964−73.
13. Pasquini J, Ceravolo R, Brooks DJ, Bonuccelli U, Pavese N. Progressive loss of raphe nuclei serotonin transporter in early Parkinson's disease: a longitudinal ^{123}I-FP-CIT SPECT study. *Parkinsonism Relat Disorders* 2020;**77**:170−5.
14. Iranzo A, Tolosa E, Gelpi E, Molinuevo JL, Valldeoriola F, Serradell M, et al. Neurodegenerative disease status and post-mortem pathology in idiopathic rapid-eye-movement sleep behaviour disorder: an observational cohort study. *Lancet Neurol* 2013;**12**:443−53.

15. Politis M, Wu K, Loane C, Turkheimer FE, Molloy S, Brooks DJ, et al. Depressive symptoms in PD correlate with higher 5-HTT binding in raphe and limbic structures. *Neurology* 2010;**75**:1920−7.
16. Luppi PH, Clément O, Valencia Garcia S, Brischoux F, Fort P. New aspects in the pathophysiology of rapid eye movement sleep behavior disorder: the potential role of glutamate, gamma-aminobutyric acid, and glycine. *Sleep Med* 2013;**14**:714−8.
17. Shao QH, Chen Y, Li FF, Wang S, Zhang XL, Yuan YH, et al. TLR4 deficiency has a protective effect in the MPTP/probenecid mouse model of Parkinson's disease. *Acta Pharmacol Sin* 2019;**40**:1503−12.
18. Grace AA, Bunney BS. The control of firing pattern in nigral dopamine neurons: burst firing. *J Neurosci* 1984;**4**:2877−90.
19. Paladini CA, Robinson S, Morikawa H, Williams JT, Palmiter RD. Dopamine controls the firing pattern of dopamine neurons *via* a network feedback mechanism. *Proc Natl Acad Sci U S A* 2003;**100**:2866−71.
20. Dawe GS, Huff KD, Vandergriff JL, Sharp T, O'Neill MJ, Rasmussen K. Olanzapine activates the rat locus coeruleus: *in vivo* electrophysiology and c-Fos immunoreactivity. *Biol Psychiatr* 2001;**50**:510−20.
21. Sharkey KA, Mawe GM. The enteric nervous system. *Physiol Rev* 2023;**103**:1487−564.
22. Li ZS, Pham TD, Tamir H, Chen JJ, Gershon MD. Enteric dopaminergic neurons: definition, developmental lineage, and effects of extrinsic denervation. *J Neurosci* 2004;**24**:1330−9.
23. Lacković Z, Relja M. Evidence for a widely distributed peripheral dopaminergic system. *Fed Proc* 1983;**42**:3000−4.
24. Singaram C, Gaumnitz EA, Torbey C, Ashraf W, Quigley EMM, Sengupta A, et al. Dopaminergic defect of enteric nervous system in Parkinson's disease patients with chronic constipation. *Lancet* 1995;**346**:861−4.
25. Volpicelli-Daley LA, Luk KC, Lee VM. Addition of exogenous α-synuclein preformed fibrils to primary neuronal cultures to seed recruitment of endogenous α-synuclein to Lewy body and Lewy neurite-like aggregates. *Nat Protoc* 2014;**9**:2135−46.
26. Neuhuber WL, Berthoud HR. Functional anatomy of the vagus system: how does the polyvagal theory comply?. *Biol Psychol* 2022;**174**:108425.
27. Sumikura H, Takao M, Hatsuta H, Ito S, Nakano Y, Uchino A, et al. Distribution of α-synuclein in the spinal cord and dorsal root ganglia in an autopsy cohort of elderly persons. *Acta Neuropathol Commun* 2015;**3**:57.
28. Spillantini MG, Schmidt ML, Lee VM, Trojanowski JQ, Jakes R, Goedert M. Alpha-synuclein in Lewy bodies. *Nature* 1997;**388**:839−40.
29. Fares MB, Jagannath S, Lashuel HA. Reverse engineering Lewy bodies: how far have we come and how far can we go?. *Nat Rev Neurosci* 2021;**22**:111−31.
30. Recasens A, Dehay B, Bové J, Carballo-Carbajal I, Dovero S, Pérez-Villalba A, et al. Lewy body extracts from Parkinson disease brains trigger α-synuclein pathology and neurodegeneration in mice and monkeys. *Ann Neurol* 2014;**75**:351−62.
31. Mahul-Mellier AL, Burtscher J, Maharjan N, Weerens L, Croisier M, Kuttler F, et al. The process of Lewy body formation, rather than simply α-synuclein fibrillization, is one of the major drivers of neurodegeneration. *Proc Natl Acad Sci U S A* 2020;**117**:4971−82.
32. Sanchez-Guajardo V, Barnum CJ, Tansey MG, Romero-Ramos M. Neuroimmunological processes in Parkinson's disease and their relation to α-synuclein: microglia as the referee between neuronal processes and peripheral immunity. *ASN Neuro* 2013;**5**:113−39.
33. Wang D, Gu X, Ma X, Chen J, Zhang Q, Yu Z, et al. Nanopolyphenol rejuvenates microglial surveillance of multiple misfolded proteins through metabolic reprogramming. *Acta Pharm Sin B* 2023;**13**:834−51.
34. Furukawa K, Shima A, Kambe D, Nishida A, Wada I, Sakamaki H, et al. Motor progression and nigrostriatal neurodegeneration in Parkinson disease. *Ann Neurol* 2022;**92**:110−21.
35. Kasanga EA, Han Y, Shifflet MK, Navarrete W, McManus R, Parry C, et al. Nigral-specific increase in ser31 phosphorylation compensates for tyrosine hydroxylase protein and nigrostriatal neuron loss: implications for delaying parkinsonian signs. *Exp Neurol* 2023;**368**:114509.
36. Good CH, Hoffman AF, Hoffer BJ, Chefer VI, Shippenberg TS, Bäckman CM, et al. Impaired nigrostriatal function precedes behavioral deficits in a genetic mitochondrial model of Parkinson's disease. *FASEB J* 2011;**25**:1333−44.
37. Maetzler W, Hausdorff JM. Motor signs in the prodromal phase of Parkinson's disease. *Mov Disord* 2012;**27**:627−33.
38. Patterson JR, Duffy MF, Kemp CJ, Howe JW, Collier TJ, Stoll AC, et al. Time course and magnitude of α-synuclein inclusion formation and nigrostriatal degeneration in the rat model of synucleinopathy triggered by intrastriatal α-synuclein preformed fibrils. *Neurobiol Dis* 2019;**130**:104525.
39. Ayers JI, Riffe CJ, Sorrentino ZA, Diamond J, Fagerli E, Brooks M, et al. Localized induction of wild-type and mutant α-synuclein aggregation reveals propagation along neuroanatomical tracts. *J Virol* 2018;**92**:e00586-18.
40. Huang CX, Zhao Y, Mao J, Wang Z, Xu L, Cheng J, et al. An injury-induced serotonergic neuron subpopulation contributes to axon regrowth and function restoration after spinal cord injury in zebrafish. *Nat Commun* 2021;**12**:7093.
41. Perrin FE, Noristani HN. Serotonergic mechanisms in spinal cord injury. *Exp Neurol* 2019;**318**:174−91.
42. den Braber-Ymker M, Lammens M, van Putten MJ, Nagtegaal ID. The enteric nervous system and the musculature of the colon are altered in patients with spina bifida and spinal cord injury. *Virchows Arch* 2017;**470**:175−84.
43. Arotcarena ML, Dovero S, Prigent A, Bourdenx M, Camus S, Porras G, et al. Bidirectional gut-to-brain and brain-to-gut propagation of synucleinopathy in non-human primates. *Brain* 2020;**143**:1462−75.
44. Xie Z, Zhang X, Zhao M, Huo L, Huang M, Li D, et al. The gut-to-brain axis for toxin-induced defensive responses. *Cell* 2022;**185**:4298−4316.e21.
45. Tysnes OB, Kenborg L, Herlofson K, Steding-Jessen M, Horn A, Olsen JH, et al. Does vagotomy reduce the risk of Parkinson's disease?. *Ann Neurol* 2015;**78**:1011−2.
46. Chandra R, Hiniker A, Kuo YM, Nussbaum RL, Liddle RA. α-Synuclein in gut endocrine cells and its implications for Parkinson's disease. *JCI Insight* 2017;**2**:e92295.
47. Holmqvist S, Chutna O, Bousset L, Aldrin-Kirk P, Li W, Björklund T, et al. Direct evidence of Parkinson pathology spread from the gastrointestinal tract to the brain in rats. *Acta Neuropathol* 2014;**128**:805−20.
48. Chen M, Mor DE. Gut-to-brain α-synuclein transmission in Parkinson's disease: evidence for prion-like mechanisms. *Int J Mol Sci* 2023;**24**:7205.
49. Tan LL, Bornstein JC, Anderson CR. Neurochemical and morphological phenotypes of vagal afferent neurons innervating the adult mouse jejunum. *Neuro Gastroenterol Motil* 2009;**21**:994−1001.
50. Schuligoi R, Herzeg G, Wachter C, Jocic M, Holzer P. Differential expression of c-fos messenger RNA in the rat spinal cord after mucosal and serosal irritation of the stomach. *Neuroscience* 1996;**72**:535−44.
51. Taché Y, Yang H, Kaneko H. Caudal raphe-dorsal vagal complex peptidergic projections: role in gastric vagal control. *Peptides* 1995;**16**:431−5.
52. Ahn EH, Kang SS, Liu X, Chen G, Zhang Z, Chandrasekharan B, et al. Initiation of Parkinson's disease from gut to brain by δ-secretase. *Cell Res* 2020;**30**:70−87.
53. Bieri G, Brahic M, Bousset L, Couthouis J, Kramer NJ, Ma R, et al. LRRK2 modifies α-syn pathology and spread in mouse models and human neurons. *Acta Neuropathol* 2019;**137**:961−80.
54. Zhao Z, Li F, Ning J, Peng R, Shang J, Liu H, et al. Novel compound FLZ alleviates rotenone-induced PD mouse model by suppressing TLR4/MyD88/NF-κB pathway through microbiota−gut−brain axis. *Acta Pharm Sin B* 2021;**11**:2859−79.

55. Jozwiak N, Postuma RB, Montplaisir J, Latreille V, Panisset M, Chouinard S, et al. REM sleep behavior disorder and cognitive impairment in Parkinson's disease. *Sleep* 2017;**40**:zsx101.
56. Monti JM. Serotonin control of sleep-wake behavior. *Sleep Med Rev* 2011;**15**:269−81.
57. Pasquini J, Ceravolo R, Qamhawi Z, Lee JY, Deuschl G, Brooks DJ, et al. Progression of tremor in early stages of Parkinson's disease: a clinical and neuroimaging study. *Brain* 2018;**141**:811−21.
58. Jellen LC, Lewis MM, Du G, Wang X, Galvis MLE, Krzyzanowski S, et al. Low plasma serotonin linked to higher nigral iron in Parkinson's disease. *Sci Rep* 2021;**11**:24384.
59. Krowicki ZK, Hornby PJ. Serotonin microinjected into the nucleus raphe obscurus increases intragastric pressure in the rat *via* a vagally mediated pathway. *J Pharmacol Exp Therapeut* 1993;**265**:468−76.
60. Eskow KL, Dupre KB, Barnum CJ, Dickinson SO, Park JY, Bishop C. The role of the dorsal raphe nucleus in the development, expression, and treatment of L-dopa-induced dyskinesia in hemiparkinsonian rats. *Synapse* 2009;**63**:610−20.
61. Wan OW, Shin E, Mattsson B, Caudal D, Svenningsson P, Björklund A. α-Synuclein induced toxicity in brain stem serotonin neurons mediated by an AAV vector driven by the tryptophan hydroxylase promoter. *Sci Rep* 2016;**6**:26285.
62. Schofield DJ, Irving L, Calo L, Bogstedt A, Rees G, Nuccitelli A, et al. Preclinical development of a high affinity α-synuclein antibody, MEDI1341, that can enter the brain, sequester extracellular α-synuclein and attenuate α-synuclein spreading *in vivo*. *Neurobiol Dis* 2019;**132**:104582.
63. Jankovic J, Goodman I, Safirstein B, Marmon TK, Schenk DB, Koller M, et al. Safety and tolerability of multiple ascending doses of PRX002/RG7935, an anti-α-Synuclein monoclonal antibody, in patients with Parkinson disease: a randomized clinical trial. *JAMA Neurol* 2018;**75**:1206−14.
64. Nordström E, Eriksson F, Sigvardson J, Johannesson M, Kasrayan A, Jones-Kostalla M, et al. ABBV-0805, a novel antibody selective for soluble aggregated α-synuclein, prolongs lifespan and prevents buildup of α-synuclein pathology in mouse models of Parkinson's disease. *Neurobiol Dis* 2021;**161**:105543.
65. Alarcón-Arís D, Pavia-Collado R, Miquel-Rio L, Coppola-Segovia V, Ferrés-Coy A, Ruiz-Bronchal E, et al. Anti-α-synuclein ASO delivered to monoamine neurons prevents α-synuclein accumulation in a Parkinson's disease-like mouse model and in monkeys. *EBioMedicine* 2020;**59**:102944.
66. Wong YC, Krainc D. α-Synuclein toxicity in neurodegeneration: mechanism and therapeutic strategies. *Nat Med* 2017;**23**:1−13.
67. Roy S, Zhang B, Lee VM, Trojanowski JQ. Axonal transport defects: a common theme in neurodegenerative diseases. *Acta Neuropathol* 2005;**109**:5−13.
68. Guo W, Stoklund Dittlau K, Van Den Bosch L. Axonal transport defects and neurodegeneration: molecular mechanisms and therapeutic implications. *Semin Cell Dev Biol* 2020;**99**:133−50.
69. Sharon O, Fahoum F, Nir Y. Transcutaneous vagus nerve stimulation in humans induces pupil dilation and attenuates alpha oscillations. *J Neurosci* 2021;**41**:320−30.
70. Bravo JA, Forsythe P, Chew MV, Escaravage E, Savignac HM, Dinan TG, et al. Ingestion of *Lactobacillus* strain regulates emotional behavior and central GABA receptor expression in a mouse *via* the vagus nerve. *Proc Natl Acad Sci U S A* 2011;**108**:16050−5.
71. Brown P, Oliviero A, Mazzone P, Insola A, Tonali P, Di Lazzaro V. Dopamine dependency of oscillations between subthalamic nucleus and pallidum in Parkinson's disease. *J Neurosci* 2001;**21**:1033−8.
72. Kühn AA, Tsui A, Aziz T, Ray N, Brücke C, Kupsch A, et al. Pathological synchronisation in the subthalamic nucleus of patients with Parkinson's disease relates to both bradykinesia and rigidity. *Exp Neurol* 2009;**215**:380−7.
73. McGregor MM, Nelson AB. Circuit mechanisms of Parkinson's disease. *Neuron* 2019;**101**:1042−56.
74. Bevan MD, Magill PJ, Terman D, Bolam JP, Wilson CJ. Move to the rhythm: oscillations in the subthalamic nucleus-external globus pallidus network. *Trends Neurosci* 2002;**25**:525−31.
75. Chen XY, Liu C, Xue Y, Chen L. Changed firing activity of nigra dopaminergic neurons in Parkinson's disease. *Neurochem Int* 2023;**162**:105465.
76. Wang Y, Zhang QJ, Liu J, Ali U, Gui ZH, Hui YP, et al. Noradrenergic lesion of the locus coeruleus increases apomorphine-induced circling behavior and the firing activity of substantia nigra pars reticulata neurons in a rat model of Parkinson's disease. *Brain Res* 2010;**1310**:189−99.
77. Szot P, Franklin A, Miguelez C, Wang Y, Vidaurrazaga I, Ugedo L, et al. Depressive-like behavior observed with a minimal loss of locus coeruleus (LC) neurons following administration of 6-hydroxydopamine is associated with electrophysiological changes and reversed with precursors of norepinephrine. *Neuropharmacology* 2016;**101**:76−86.
78. Comai S, Ochoa-Sanchez R, Dominguez-Lopez S, Bambico FR, Gobbi G. Melancholic-like behaviors and circadian neurobiological abnormalities in melatonin MT1 receptor knockout mice. *Int J Neuropsychopharmacol* 2015;**18**:pyu075.
79. Pal D, Mallick BN. Neural mechanism of rapid eye movement sleep generation with reference to REM-OFF neurons in locus coeruleus. *Indian J Med Res* 2007;**125**:721−39.
80. Matschke LA, Komadowski MA, Stöhr A, Lee B, Henrich MT, Griesbach M, et al. Enhanced firing of locus coeruleus neurons and SK channel dysfunction are conserved in distinct models of prodromal Parkinson's disease. *Sci Rep* 2022;**12**:3180.
81. Zhu J, Yang LK, Chen WL, Lin W, Wang YH, Chen T. Activation of SK/K_{Ca} channel attenuates spinal cord ischemia−reperfusion injury *via* anti-oxidative activity and inhibition of mitochondrial dysfunction in rabbits. *Front Pharmacol* 2019;**10**:325.
82. Dolga AM, de Andrade A, Meissner L, Knaus HG, Höllerhage M, Christophersen P, et al. Subcellular expression and neuroprotective effects of SK channels in human dopaminergic neurons. *Cell Death Dis* 2014;**5**:e999.
83. Paladini CA, Williams JT. Noradrenergic inhibition of midbrain dopamine neurons. *J Neurosci* 2004;**24**:4568−75.
84. Ferrucci M, Giorgi FS, Bartalucci A, Busceti CL, Fornai F. The effects of locus coeruleus and norepinephrine in methamphetamine toxicity. *Curr Neuropharmacol* 2013;**11**:80−94.
85. Prasuhn J, Prasuhn M, Fellbrich A, Strautz R, Lemmer F, Dreischmeier S, et al. Association of locus coeruleus and substantia nigra pathology with cognitive and motor functions in patients with Parkinson disease. *Neurology* 2021;**97**:e1007−16.
86. Fornai F, Torracca MT, Bassi L, D'Errigo DA, Scalori V, Corsini GU. Norepinephrine loss selectively enhances chronic nigrostriatal dopamine depletion in mice and rats. *Brain Res* 1996;**735**:349−53.
87. Zuscik MJ, Sands S, Ross SA, Waugh DJ, Gaivin RJ, Morilak D, et al. Overexpression of the α_{1B}-adrenergic receptor causes apoptotic neurodegeneration: multiple system atrophy. *Nat Med* 2000;**6**:1388−94.
88. Pickel VM, Joh TH, Reis DJ. A serotonergic innervation of noradrenergic neurons in nucleus locus coeruleus: demonstration by immunocytochemical localization of the transmitter specific enzymes tyrosine and tryptophan hydroxylase. *Brain Res* 1977;**131**:197−214.
89. Ortega JE, Mendiguren A, Pineda J, Meana JJ. Regulation of central noradrenergic activity by 5-HT3 receptors located in the locus coeruleus of the rat. *Neuropharmacology* 2012;**62**:2472−9.
90. Mateo Y, Ruiz-Ortega JA, Pineda J, Ugedo L, Meana JJ. Inhibition of 5-hydroxytryptamine reuptake by the antidepressant citalopram in the locus coeruleus modulates the rat brain noradrenergic transmission *in vivo*. *Neuropharmacology* 2000;**39**:2036−43.
91. Segal M. Serotonergic innervation of the locus coeruleus from the dorsal raphe and its action on responses to noxious stimuli. *J Physiol* 1979;**286**:401−15.

92. Delaville C, Navailles S, Benazzouz A. Effects of noradrenaline and serotonin depletions on the neuronal activity of globus pallidus and substantia nigra pars reticulata in experimental parkinsonism. *Neuroscience* 2012;**202**:424−33.
93. Vilas D, Iranzo A, Pont-Sunyer C, Serradell M, Gaig C, Santamaria J, et al. Brainstem raphe and substantia nigra echogenicity in idiopathic REM sleep behavior disorder with comorbid depression. *J Neurol* 2015;**262**:1665−72.
94. MacGillivray L, Reynolds KB, Sickand M, Rosebush PI, Mazurek MF. Inhibition of the serotonin transporter induces microglial activation and downregulation of dopaminergic neurons in the substantia nigra. *Synapse* 2011;**65**:1166−72.